Design and Implementation of IGBT Based Power Supply for Food Treatment

by

Mohammad Saleh Moonesan

A thesis
presented to the University of Waterloo
in fulfillment of the
thesis requirement for the degree of
Master of Applied Science
in
Electrical and Computer Engineering

Waterloo, Ontario, Canada, 2011

AUTHOR'S DECLARATION

I hereby declare that I am the sole author of this thesis. This is a true copy of the thesis, including any required final revisions, as accepted by my examiners.

I understand that my thesis may be made electronically available to the public.

Abstract

Pulsed electric field (PEF) processing has been demonstrated to be an effective non-thermal pasteurization method for food-treatment applications. With this method, high voltage, short-duration pulses are applied to a chamber through which liquid food is passed. If the voltage applied and the corresponding electric field develops a potential higher than a critical trans-membrane potential, the pores expand, and the membrane of the living cell is ruptured. Due to the lower amount of energy consumed during a PEF process, the temperature of the liquid is kept much lower than as opposed to conventional pasteurization. The PEF method thus kills bacteria and other microorganisms while preserving the nutrition and taste of the liquid foods.

Although the parameter responsible for inactivation is the voltage applied, for any given voltage, the conductivity of the liquid defines a current through the liquid that causes the temperature to rise. Therefore, preventing excessive heating of the liquid requires the application of an efficient waveform. According to the literature, the most efficient waveform is a square wave since the entire energy applied would be used for the inactivation process. Although some power supplies are capable of generating such a waveform, the generation of an efficient waveform that satisfies all the requirements for producing a viable product for PEF applications is still a challenging problem.

In this research, a cascadable pulse generator, based on a Marx generator design, was designed and implemented in order to generate a pulsed waveform for the treatment of liquid food. IGBT switches were used to charge capacitors in parallel and to discharge them in series as a means of generating a high voltage at the output. The design was implemented and tested for two stages, generating up to 6 kV and 1.6 kA square pulses with a controllable pulse width from 1 μs to 10 μs. Up to 3 switches were connected in parallel to enhance the current capability of the system. Also investigated are ways to improve the transient time by enhancing the IGBT driver circuit. The effect of design parameters such as pulse width, voltage, and current on the temperature rise in the liquid was also studied. A variety of liquid foods with different conductivities were tested in order to confirm the functionality of the system.

Acknowledgements

First and foremost, I like to thank my supervisor, Professor Shesha Jayaram for her great guidance and kind support throughout my graduate studies. Her approach and teaching has inspired me to continue my graduate studies.

My deepest gratitude goes to all the members of my family, for the wonderful support they all provided; specially me wife, Desireh Shojaei-Asanjan, my mother, Shamsi Mahve Bidokhti, my father, Mohammad Taghi Moonesan, my mother in law, Dr. Parisa Derakhshan Moghaddam, and my father in law, Behrouz Shojaei-Asnajn.

I would like to thank Dr. Magdy Salama and Dr. Ramadan El-Shatshat for reviewing my thesis and also Dr. Mehrdad Kazerani for his guidance and advice throughout this work.

I would also like to thank my friends in high voltage engineering laboratory at the University of Waterloo: Ahmed, Chitral, Emad, Michael, Omar, Refat, Suat, Susan, Utkrash, you all contributed to my learning experience. Special thanks to Jian Feng Zhang (Michael) because of his help during lab experiments.

My thanks go to my all dear friends who have enriched my life. I would also like thank my friend Mohammad Reza Fakhari Arani for his help.

The financial support provided by NSERC of Canada is also greatly appreciated.

Dedication

To my dear wife and beloved parents.

Table of Contents

AUTHOR'S DECLARATION ii
Abstract iii
Acknowledgements iv
Dedication v
Table of Contents vi
List of Figures viii
List of Tables xii
Chapter 1 Introduction 1
1.1 Background 1
1.1.1 Pulse Electric Field 1
1.2 PEF Technology in the Literature 2
1.2.1 Applications of PEF for Semi-Liquid and Solid Foods 5
1.3 Power supplies for PEF 9
1.4 Motivation 13
1.5 Objectives 13
Chapter 2 System Design 15
2.1 Measurement System 15
2.2 Treatment Chamber 15
2.3 Switches 16
2.4 Voltage Requirements 19
2.5 Current Requirements 19
2.6 Voltage Waveform 20
2.7 Energy Requirements 21
2.8 Circuit Design 22
2.9 Design Parameters 25
2.10 DC input voltage stage 27
Chapter 3 Trigger Unit Design 29
3.1 Introduction 29
3.2 IGBT Driver ICs 31
3.2.1 TD351 Driver Chip 31
3.2.2 TC4421 Driver Chip 32

3.2.3 MIC4451 Driver Chip 32
3.3 Trigger Circuit Design 33
3.4 Driver Circuit Power Supply 38
Chapter 4 Controller Unit 40
4.1 Microcontroller 41
4.2 LCD 43
4.3 Keypad 44
4.4 Protection Circuit 44
4.5 Firmware 45
4.5.1 Pulsed Waveform Generation 46
Chapter 5 Results and Discussion 47
5.1 Trigger Signal 47
5.2 Output Waveform 48
5.3 Rise and Fall Times 53
5.4 Effect of Pulse Width on Temperature Rise 57
5.5 Eliminating the Noises 62
Chapter 6 Conclusion and Future Works 66
6.1 Summary and Conclusion 66
6.2 Future Work 68
Bibliography 69

List of Figures

Figure 1.1. Breakdown of a microbial cell, showing compression by electromechanical force due to the application of the electric field. The membrane acts as a capacitor shown by the hatched area; Ec is the critical electric field; (a) normal cell membrane; (b) membrane compression; (c) pore formation with reversible breakdown; (d) large pore formation with irreversible breakdown [2, 4]. 2
Figure 1.2. Block diagram of PEF application during apple juice extraction [25]. 6
Figure 1.3. Schematic circuit of a magnetic pulse generator [44]. 10
Figure 1.4. PEF generator using an H-bridge and pulse transformer [48]. 11
Figure 1.5. Schematic of a solid state Marx generator for food treatment taken from [49]. 12
Figure 1.6. Schematic of Diversified Technologies Inc. solid state generator for food treatment [51]. 12
Figure 2.1. Treatment chamber showing the electrode spacing and the uniformity of the treatment zone. 16
Figure 2.2. Voltages, currents, and frequency capabilities of different types of power electronics semiconductor switches [60]. 17
Figure 2.3. IXBX55N300 specifications [61]. 18
Figure 2.4. CM600HA-24A package [62]. 18
Figure 2.5. Living cell under application of electric field [63]. 19
Figure 2.6. Energy dissipation in a decaying impulse waveform. 21
Figure 2.7. Generator schematic [66]. 22
Figure 2.8. Schematic of a solid state Marx generator. 23
Figure 2.9. Equivalent circuit of the charging cycle. 23
Figure 2.10. Equivalent circuit of the discharging cycle. 24
Figure 2.11. Test setup with two stages and two switches in parallel in each stage. 25
Figure 2.12. Input stage circuit including the AC input and rectifier for generation of input DC high voltage. 28
Figure 3.1 Block diagram of the triggering system. 29
Figure 3.2. Schematic of the interlock block. 30
Figure 3.3. Fiber optic transmitter and receiver. 30
Figure 3.4. Typical schematic and internal block diagram of the TD351 driver chip [67]. 31
Figure 3.5. Block diagram of the TC4421 driver chip [68]. 32
Figure 3.6. Internal block diagram of the MIC4451 driver chip [69]. 33

Figure 3.7. IGBT model showing input, output, and reverse transfer capacitances; C_{GE} = gate emitter capacitance, C_{GC} = gate collector capacitance and C_{CE} = collector emitter capacitance. 33
Figure 3.8. The variations in the dynamic capacitances relative to the V_{CE} [61]. 34
Figure 3.9. The variation of the gate-source voltage relative to the total gate charge Q_G [70]. 34
Figure 3.10. V_{GE} - Q_G curve of the IXBX55N300 [61]. 35
Figure 3.11. Gate voltage and current of the IXBX55N300 (left) and the CM600HA24A (right) driven by the MC4451 (12 A) chip; Voltage: CH3, 5 V/div; Current: CH2, 50 mv/A;Time 500 ns/div. 36
Figure 3.12. Schematic of enhanced IGBT driver circuit [71]. 37
Figure 3.13. Schematic of the driver circuit power supply used by Yu[66]. 39
Figure 4.1. Block diagram of the controller unit. 40
Figure 4.2. PIC16F877 microcontroller block diagram [72]. 42
Figure 4.3. LCD read and write timing. 43
Figure 4.4. Block diagram of the LCD. 44
Figure 4.5. 4 by 4 keypad configuration. 44
Figure 4.6. Flow chart of the firmware program. 45
Figure 4.7. Block diagram of timer 0 46
Figure 5.1. IGBT gate voltages for charging (CH1, Orange) and discharging (CH3, Purple); voltage: CH1 5 V/div; current: CH3 5 A/div; time: 10 µs/div. 47
Figure 5.2. Waveform with output voltage (CH1: 2 kV/div) and current (CH3: 500 A/div) for 2 switches in parallel and a 2-stage configuration for different pulse widths: 3.5 µs (left); 5.8 µs (right); time 1µs/div. 48
Figure 5.3. Voltage and current waveform of the Ohio State University pulse generator [48]. 49
Figure 5.4. Voltage and current waveform of the pulse generator developed by Cheng et al. based on a flyback converter [45]. 49
Figure 5.5. Voltage and current waveform of the pulse generator developed by Beak et al. based on a solid state Marx generator [49]. 50
Figure 5.6. Output voltage waveform of the pulse generator developed by Grenier et al. based on MOSFETs in series [46]. 50
Figure 5.7. Output voltage waveform of Diversified Technologies's pulse generator based on IGBTs in series [52]. 51

Figure 5.8. Output voltage waveform of an IGBT driven by an enhanced driver circuit, developed by Nguyen et al. [71]. 51
Figure 5.9. Output voltage waveform of a pulse generator based on a magnetic compressor [44]. 52
Figure 5.10. Output waveform of the generator with a 4.4 Ω load in 5.8 kV with large pulse widths (a) 10 μs (b) 5 μs; voltage: CH1 1 kV/div; current: CH3 200 A/div, CH4 100 A/div; time: 2.5 μs/div... 53
Figure 5.11. Output voltage (CH1) and current (CH3) waveform for 2 switches in parallel and a 2-stage configuration for different load conductivities: (a) 200 μS/cm voltage: CH1 2 kV/div, current: CH3 50 A/div(b) 1000 μS/cm voltage: CH1 2 kV/div, current: CH3 100 A/div (c) 3300 μS/cm voltage: CH1 1 kV/div, current: CH3 500 A/div (d) 15 000 μS/cm voltage: CH1 200 V/div, current: CH3 500 A/div; time: 500ns/div. 54
Figure 5.12. Rise times under different conductivities and configurations (SW = number of switches in parallel; ST = number of stages). 54
Figure 5.13. Fall times under different conductivities and configurations (SW = number of switches in parallel; ST = number of stages). 55
Figure 5.14. Rise times with different configurations under load conductivity (a) 200 μS/cm and (b) 15 000μS/cm. 56
Figure 5.15. Changing rise and fall times with different load conductivities for 2 kV on a configuration with 3 switches and 1 stage. 56
Figure 5.16. Comparison of the IXBX55N300 (3 kV, 55 A IGBT) and the CM600HA-24A (1.2 kV, 600 A IGBT) with respect to rise/fall times with different load conductivities. 57
Figure 5.17. Temperature rise in alcoholic apple cider during 30 seconds with the application of 5.1 kV, 1 kA, and 3 Hz pulses with a 3.5 μs width (LI01 and LI02 represent the temperature measurement lines). 59
Figure 5.18. Temperature rise (ºC) in alcoholic apple cider during 30 seconds with the application of 5.1 kV, 1 kA, and 3 Hz pulses with a 3.5 μs width (each line represents one of the spots on the chamber; each horizontal point represents 0.4s). 59
Figure 5.19. Temperature rise at each point of the chamber. 60
Figure 5.20. Temperature rise in apple cider with respect to time along the measurement lines (Blue = LI01; Red = LI0). 60
Figure 5.21. Temperature rise in the liquid with respect to pulse width. 62
Figure 5.22. Unexpected oscillations on the waveform causing the system failure. 62
Figure 5.23. Replacing high voltage wires with copper strips to eliminate oscillations. 63

Figure 5.24. Unexpected oscillations during the rise state of the waveform with voltage levels higher than 3.5 kV and with two stages, causing system failure. 63
Figure 5.25. Shielding the IGBT driver circuit in order to reduce noise. 64
Figure 5.26. Shielding the power supply of the driver circuit in order to reduce noise. 64
Figure 5.27. Ground loop current in the driver circuit [74]. 65

List of Tables

Table 1.1. Inactivation levels using different pulse application schemes [4]. 3
Table 1.2. Liquid egg treatment conditions [28]. 8
Table 2.1. CM600HA-24A specifications [62]. 18
Table 2.2. Conductivity of liquid foods and their equivalent resistance in the treatment chamber with 1.27 mm gap. 20
Table 2.3. The design parameters. 25
Table 3.1. A comparison on the various parameters of the driver chips. 31
Table 3.2. Input, output, and reverse transfer capacitance of IXBX55N300; Cies = input capacitance, i.e. Cies= CGS + CGC , output capacitance Coes= CGC + CCE ; and reverse transfer capacitance Cres= CGC [61]. 33
Table 3.3. Comparison of the rise and fall times of two switches with respect to the driver circuit current under different conductivities. 36
Table 3.4. Effect of the number of driver chips in parallel on the rise and fall times for the CM600HA-24A. 37
Table 4.1. PIC16F877A specifications. 41
Table 4.2. PIC microcontroller chip pin connections. 41
Table 5.1. Rise and fall times under different conductivities and configurations. 55
Table 5.2. Measured total time and energy per pulse for different pulse widths. 61

Chapter 1
Introduction

Compared to pasteurization, a pulsed electric field (PEF) is as effective in killing bacteria and other microorganisms but performs better with respect to preserving the taste and nutritional value of liquid food. PEF destroys microorganisms when the voltage applied and its corresponding electric field develops a potential higher than a critical trans-membrane potential, which breaks the membrane of the living cell by expanding the existing pores [1]. The cell contents diffuse into their surroundings, and the metabolic pathways then attain a thermal equilibrium that causes the death of the living cell. Due to the lower amount of energy consumed during the PEF process, the temperature of the liquid is kept low, in contrast to the conventional pasteurization method, in which the temperature of the liquid is about 70ºC.

PEF can also increase the efficiency of the extraction process for semi-liquid foods, such as the extraction of sugar from beetroot or the yielding of juice from grape or apple tissues. PEF has therefore attracted the interest of the food industry as a means of producing higher-quality food products. The aim of this research is to develop a power supply suitable for use in PEF food-treatment applications.

1.1 Background

This section provides information about the basic principles of the PEF method used to inactivation of microorganisms and previous related research.

1.1.1 Pulse Electric Field

Applying a pulse electric field to a living cell results in a change in the permeability of the cell membrane. This process, known as electroporation, can be either reversible or non-reversible. Reversible processes can be used in drug-delivery applications while non-reversible electroporation is useful for treatment or extraction applications. Some studies have been directed at furthering an understanding of the electroporation mechanism. One theory proposed is that pores are formed in the cell membrane due to the instabilities caused by electromechanical and electric-field-induced compression. In fact, the electric field creates an accumulation of positive and negative charges at two

sides of the cell membrane, causing compression of the cell [2]. If a critical amount of potential, about 0.75 V-1.25 V, is applied to a living cell, compression results in the thickness of the membrane decreasing and becoming permeable to its surrounding medium, which causes the cell membrane to break down [1, 3].

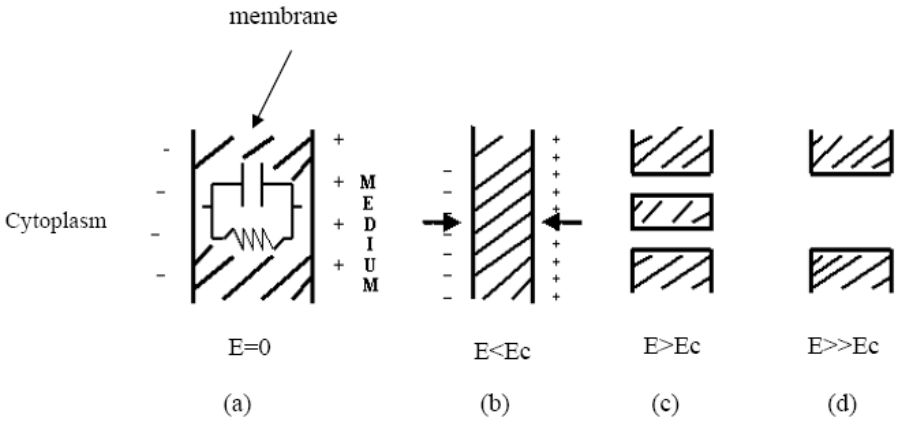

Figure 1.1. Breakdown of a microbial cell, showing compression by electromechanical force due to the application of the electric field. The membrane acts as a capacitor shown by the hatched area; Ec is the critical electric field; (a) normal cell membrane; (b) membrane compression; (c) pore formation with reversible breakdown; (d) large pore formation with irreversible breakdown [2, 4].

The theory of osmotic imbalance suggests that some ions and small molecules escape from the pores produced by the electric field and cause an osmotic imbalance and enlargement of the cell until the cell bursts [5]. The theory of electroporation has been reviewed in the literature [6, 7].

1.2 PEF Technology in the Literature

Many studies have been conducted with respect to the use of PEF as a method of non-thermal food treatment, some of which are referred to in this thesis.

Hienz et al. [8] used 1.8 kV/mm to 4.2 kV/mm and 40 kJ/kg to 160 kJ/kg energy to treat apple juice at temperatures ranging from 35º C to 56º C using an exponential decay impulse to achieve the inactivation level of 3-9 log cycles. They showed that at higher temperatures PEF results in higher level of inactivation. However in their work, the temperature of the liquid reached as high as 65º C, making it difficult to judge whether the killing was non-thermal or thermal. Keeping the temperature of the liquid below 40º C, is important because of the effect of elevated temperature on the nutrients [9, 10].

Shamsi et al. [4] reviewed applications of PEF in the non-thermal processing of milk. They studied a number of parameters that affect the PEF and provided a table that compares the parameters and the results. Table 1.1 shows a portion of their comparison.

Table 1.1. Inactivation levels using different pulse application schemes [4].

Microorganisms	Treatment medium	E (kV/cm)	T (°C)	Log reduction
E. coli	SMUF	36 & 60	40	6.0 & 9.0
L. monocytogenes	Milk	25 & 35	25 50	1-4.0
L. innocua	Skim milk	30, 40 & 50	22 28 34	1.7, 2.0 & 2.5
E. coli *L. innocua*	Skim milk	41	37	2.3-4.0 & 0.7-3.9
L. innocua	Whole milk	29	35.5	1.13
P. fluorescens	SMUF	16.4 & 37.3	50 90	Various
L. lactis	Skim milk	35	52	3.0
L. monocytogenes	Skim milk	15 &30	<50 55	1- 4.5
E. coli O157:H7	Skim milk	24	30	2.0, 1.27 & 1.88
Pseudomonads	UHT milk		15 40 45 55	3.1
Enterobacteriaceae				2.4
Pseudomonads	Skim milk	25-37	15 & 60	5.9

According to the above table, experiments show that the best results can be achieved using an electric field strength of 3.6 kV/mm to 6 kV/mm and a temperature of 40º C. Inactivation as high as 9 log reductions has been reported with the use of a continuous chamber and a 40 µs treatment time. It should be noted that a lower electric field results in substantially lower inactivation.

El-Hag et al. [11] used PEF to inactivate naturally grown bacteria in orange juice. They applied 120 pulses/mL of a decaying impulse waveform at a field level of 4.6 kV/mm and reported an inactivation level of 2 log reductions. They noticed that increasing the operation temperature by 20º C enables an increase in inactivation by 1 log reduction.

Samperdro et al. [12] used a 3.5 kV/mm to 4 kV/mm field and 2.5 µs and 4 µs pulse widths to treat orange juice-milk based beverage using different energy levels. They reported an inactivation level of

1.5 log reductions when 200 kJ/L to 285 kJ/L of energy were applied and noticed small changes in inactivation when the energy applied was increased to 813 kJ/L to 891 kJ/L. They continued to increase the energy to 1069 kJ/L to 1170 kJ/L and reported a log reduction of 2. Such an energy level is relatively high and could initiate thermal processes. It seems that, an energy level of 200 kJ/L would be the most efficient level.

Salvia-Trujillo et al. [13] compared PEF and thermal pasteurization for treating fruit juice-milk beverages. They used 3.5 kV/mm, 200 Hz, and 4 μs square pulses to treat the liquid below 40º C. They reported 5 log reductions after an 1800 μs treatment. The results demonstrate that, in both methods, the beverages show microbial stability over 56 day period at 4º C with very small changes in pH, acidity, and soluble solid contents. However, the thermal method results in more inactivation in pectin methyl esterase (PME) and polygalacturonase (PG) activity. The authors claimed that PEF is a feasible method for achieving shelf-stable fruit juices with better quality.

Luo et al. [14] used the same principle as in [13] to compare the shelf life of carrot juice using PEF treatment with 2.5k V/mm and 200 μs compared with pasteurization at 95º C for 15 seconds. Although the effectiveness of inactivation using PEF for PME was lower than with the thermal method, for 28 days at 4º C, PEF maintained microbial stability as well as color and turbidity, in contrast to the thermal process, in which a number of changes have been observed in regard to these aspects.

Pataro et al. [15] reported 7 log reductions using 3 kV/mm pulses with 110 J/mL of energy, having a flow rate of 2 L/h. They concluded that faster stirring can help save energy and produce higher inactivation and also that continuous treatment is more effective than using a batch mode.

Gurtler et al. [16] combined preservatives such as sodium benzoate, potassium sorbate, and 2.7 % citric acid with PEF with a level of 1.8 kV/mm for 150 μs at temperatures of 45º C to 55º C. They reported inactivation of 2-7 log reductions. At the highest point, they achieved 7 log reductions. However, it seems that they used a small field level and relatively high temperatures.

References [17, 18] reported the migration of metal parts from the electrode to the liquid during the use of PEF. The electrode material is one of the affecting parameters that should be considered in PEF applications.

Qin et al. [19] achieved 6 log reductions during the treatment of apple juice using PEF. The treatment conditions were 10 pulses of 2.5 μs and 3.5 kV/mm and 2 pulses of 2.5 μs and 5 kV/mm with the temperature kept below 30º C. In both cases, the shelf life was increased to about 3 weeks.

Zhang et al. [20] compared a square waveform and a decaying impulse waveform for treating apple juice with the same voltage and energy input. The results showed that the square waveform is more effective than the impulse.

References [21] and [22] have reviewed and summarized the research which has been conducted with respect to PEF technology.

1.2.1 Applications of PEF for Semi-Liquid and Solid Foods

Liquid food products, such as water, juices, milk, and beer can be treated using the PEF method. The systems used employ a pump to circulate the liquid through a chamber. However, the use of this method for the treatment of semi-liquid or solid food is still a challenging problem because in the traditional setup, the waveform applied, and the power rating are not appropriate for the treatment of semi-liquid or solid foods. Experiments have been conducted with respect to the treatment of semi-liquid foods, such as liquid egg, cheese whey, and also for the treatment of some solid foods, such as apple tissue, potato tissue, and muscle foods. The PEF method has also been used to extract sucrose from sugar beets and for the treatment of red beetroot pigment. In both applications, the food is semi-liquid during the extraction process.

The application of PEF for semi-liquid and solid food can be divided into two main categories: the enhancement of the extraction process for semi-liquid and solid foods using PEF, and the treatment of solid or semi- liquid food using PEF. The following sections explain the use of the PEF method for these categories.

1.2.1.1 Enhancement of the Extraction Process in Liquid- Solid Foods Using PEF

Sack et al. [23] used a PEF device to produce wine from mashed grapes. A Marx generator was employed to apply a 3.6 kV/mm field strength with a pulse duration of 1.1 μs, 20 Hz, and specific energy of 34.2 kJ/kg at 20º C. Mashed grapes was pumped with a constant flow rate of 900 L/h for treatment. The result were compared with the conventional thermovinification process, in which the mash is heated up to 80º C, kept at that temperature for 2 minute, and then cooled down to less than 40º C. The estimated specific energy for thermovinification is 205 kJ/kg when the temperature is

raised by 60 degrees. The temperature rise is significantly higher with the thermal method than that of using the PEF method which is about 30 degrees.

Chalermchat et al. [24] conducted experiments with the goal of enhancing the yield percentage of solid-liquid potato tissues using PEF. Potatoes were cut into cylindrical pieces with a diameter of 6.3 mm and a thickness of 4.4 mm. A 68 V/mm electric field strength with a duration of 100 μs and a frequency of 50 Hz used to perform the treatment process. To increase the efficiency of yielding process, PEF and pressure were applied at the same time. The yielding percentage was increased by 10.

Bazhal et al. [25] used PEF during compression for apple juice extraction. They used a high voltage pulse generator with a rating of 1500 V, 15 A to apply pulses to the apple tissues during compressing process. The pulses had a duration of 100 μs at 100 Hz and a field of about 10 V/mm to 52 V/mm. The results show that applying high pressure to the apple tissues helps decrease conductivity and therefore the effectiveness of PEF for extraction. Fig. 1.2 shows the block diagram of the design.

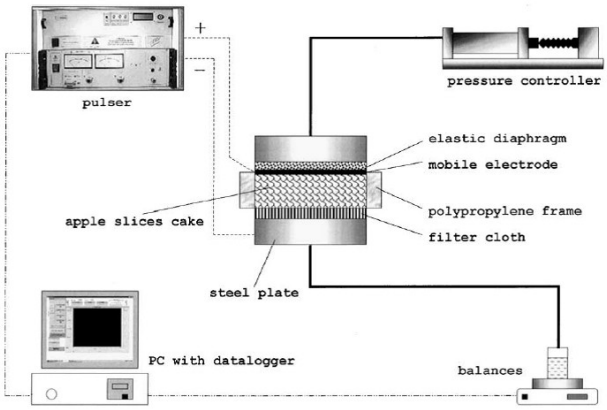

Figure 1.2. Block diagram of PEF application during apple juice extraction [25].

Fincan et al. [26] tried to enhance the extraction of red pigment from red beetroot using PEF-treated tissues. They achieved a higher degree of extraction with PEF than with either freezing or mechanical pressing. They used 270 rectangular pulses of 10 μs at 100 V/mm field strength, with an energy consumption of 7 kJ/kg. The results showed that the, samples released about 90 % of total red colouring during 1 hour of extraction.

Lopez et al. [27] worked on the enhancement of the semi-liquid extraction of sucrose from sugar beets using PEF. The following specifications were used to investigate the sucrose extraction from

sugar beets at different temperatures, ranging from 20º C to 70º C: 0.1 kV/mm to 0.7 kV/mm, 5-40 pulses, 0.006 kJ/kg to 0.19 kJ/kg per pulse, at 1 Hz to 10 Hz, and a pulse width of 2 ms to 5 ms, with square and exponential decay pulses. However, the efficiency of the solid-liquid extraction was independent of the frequency, pulse width, and pulse shape at 0.7 V/mm; it was affected by the strength of the electric field applied and by the temperature of the extracting medium. The application of 20 pulses at 0.7 kV/mm with an energy of 3.9 kJ/kg increased the maximum yield by 7 and 1.6 times, compared with non-PEF-treated samples, at 20º C and 40º C, respectively.

1.2.1.2 Treatment of Solid and Semi-Liquid Foods Using PEF

Sampedro et al. [28] reviewed the literature related to the application of PEF for eggs and egg derivatives. Table 1.2 shows a summary of the work reviewed. Most of the studies used a pulse width between 1 μs and 4 μs, and an applied field of 1.5 kV/mm to 5 kV/mm. Generally, the methods that used heat in addition to the PEF treatment have smaller fields. Unfortunately, in these studies, the amount of energy applied is not indicated except in one case, in which a 2.6 kV/mm field with a 2 μs to 4 μs pulse width and energy of 60 J to120 J was used. Considering the frequency, liquid flow and number of pulses applied, they applied 12 J/mL and achieved a log reduction level of 5 for the E-coli microorganism. The temperature of the liquid was 37º C, which seems relatively low compared with other cited works.

In another investigation of liquid egg, Amiali et al. [29] proposed a test setup for inactivating E-coli O157:H7 in egg white, egg yolk, and whole egg using pulse electric field. They used 1.5 kV/mm and 500 pulses of 1 Hz with a 200 μs duration. The results showed that egg white requires more energy to inactivate than whole egg or egg yolk. The energy density required to treat egg yolk was much lower than that needed to treat egg white or whole egg. They reported applying 3080 kJ/L of energy in order to achieve 3.1 log reductions in egg yolk, while using 5210 kJ/L of energy to obtain only 1.2 log reduction for whole egg.

Monfort et al. [30] also conducted studies using liquid egg. The results of their investigation seem closer to reality. In their work, maximum inactivation levels of 4 and 3 log cycles for Salmonella Typhimurium and S. aureus were achieved with treatments of 4.5 kV/mm for 30 μs and 419 kJ/kg and of 4 kV/mm for 15 μs and 166 kJ/kg, respectively. They concluded that treatments higher than 200 kJ/kg to 250 kJ/kg produce a negligible increase in the lethal effectiveness of the process. They proposed that better results can be obtained by limiting the energy to 200 kJ/kg to 250 kJ/kg and by combining the PEF method with another treatment technology. The amount of energy used for the

treatment of liquid egg in this investigation is more feasible than that used in the one conducted by Amiali et al.

Table 1.2. Liquid egg treatment conditions [28].

Source	Type of Sample	Type of Microorganism	Log Reduction	Equipment and Process Conditions
Martín-Belloso et al. (1997)	LWE	*E. coli*	5–6 E = 26 kV/cm, T = 37.2 °C	Continuous, d = 0.6 cm, E = 26 kV/cm, W = 2–4 μs, T = 37 °C, 1.25–2.5 Hz, 0.5 L/min, 0.5–1 μF, 60–120 J two treatments: 1. Continuous circulation: 0, 10, 20, 40, 60, 80 and 100 pulses 2. Stepwise treatment: five steps of 20 pulses/step *Laboratory-Size Prototype WSU*
Calderón-Miranda et al. (1999)	LWE	*L. innocua*	3.4 (50 kV/cm and 32 pulses) 0.53 (nisin 100 IU/mL) 5.5 50 kV/cm and 32 pulses + nisin 100 IU/mL	Continuous, exponential, d = 0.6 cm, E = 30, 40, 50 kV/cm, W = 2 μs, N = 10.6, 21.3, 32 pulses, 0.5 L/min, 3.5 Hz, T = 26–36 °C *Pilot Plant System WSU*
Góngora-Nieto et al. (1999)	LWE	*P. fluorescens* (WSU-07, ATCC 17400, ATCC 13525)	90% (PEF or HHP + citric acid) 90% (WSU-07) 4 (ATCC17400 and 13525)	PEF/HHP alone or combined with antimicrobials PEF (130 pulses and E = 38 kV/cm) HHP (5 min and 20–40 Kpsi) *Pilot Plant System WSU*
Jeantet et al. (1999)	Egg white diaultrafiltered	*S. enteritidis*	3.5 PEF E = 35 kV/cm, 900 Hz, 8 pulses, T = 30 °C Heat 55 °C, 15 min	*PEF* Batch, exponential, monopolar, V = 400 μL, d = 0.2 cm, 100–900 Hz, T = 4–30 °C, E = 20–35 kV/cm, N = 2–8 pulses, pH = 7–9 Heat T = 55 °C, 3, 6, 9, 12 and 15 min *Modified Thomson-CSF Generator, Gene Pulser Chambers*
Hermawan et al. (2004)	LWE and model solution	*S. enteritidis*	1 PEF 4.3 PEF + 55 °C, 3.5 min	Continuous, 200 pps, 1.2 mL/s, E = 25 kV/cm, W = 2.12 μs, time = 250 μs *OSU-3C*
Amiali et al. (2004)	LWE, egg yolk, and egg white, all dialysed	*E. coli*	3.5 (whole egg) 2.9 (egg yolk) 1 (egg white)	Batch, E = 15 kV/cm, negative square waveform, time = 200 μs, 0.23 mL, d = 0.15 cm, S = 1.53 cm^2, 1 Hz and N = 100, 200, 300 and 500 pulses
Jeantet et al. (2004)	Model solution and egg white ultrafiltered pH = 6 and pH = 9 with 0.45% lysozyme added	*S. enteritidis*	4 (model solution) 2 (egg white, pH = 6 and 9)	Continuous, 0–25 L/h, E = 30–80 kV/cm, W = 50 ns–3 μs, 10–815 Hz
Bazhal et al. (2006)	LWE	*E. coli* 0157:H7	1 (20–50 °C) 4 min 4 (65 °C) 4 min 2.5 PEF (9–15 kV/cm) + HEAT (55 °C) 4 PEF (15 kV/cm) + HEAT (60 °C)	Batch, E = 9–15 kV/cm, 2 mL, d = 1 cm, bipolar square waveform, N = 138 pulses, 1 Hz, W = 2 μs

Alvarez et al. [31] investigated the effect of the electric field strength, the treatment time, the total specific energy, and the conductivity of the treatment medium on the inactivation of Listeria monocytogenes PEF. A maximum inactivation of 4.77 log cycles was reported after a treatment with 2.8 kV/mm, 2000 μs, and 3490 kJ/kg of energy. This amount of the energy causes a rise in temperature in the medium, and as a result, this method is less beneficial than the pasteurization process. The treatment time and specific energy were at the normal values reported in the literature for treatment, but the specific energy was at a very high order in this investigation. An interesting note is that, this result is near to what obtained in the above mentioned investigation of liquid egg by Amiali et al. [29].

Gallo et al. [32] researched the use of a combination of PEF and nisin (a polycyclic antibacterial) to inactivate bacteria in cheese whey. They used an exponential decay pulse generator to deliver 60 pulses at 1.2 kV/mm to the load. They seem to have applied about 1300 J/mL to inactivate the

bacteria, which is reasonable but still seems high relative to the reduction and taking into account the help provided by the nisin. The research shows that a combination of PEF and nisin can be an effective method of inactivating bacteria in cheese whey.

Gudmundsson et al. [33] conducted research on the effect of PEF and a combination of PEF and high pressure. They studied the microstructure of salmon, chicken, and lumpfish roe. The results showed that PEF treatment with a low field strength (less than 2 kV/cm and 20-40 pulses) had considerable effect on the microstructure. A decrease in the size and gaping of the muscle cells were reported. PEF treatment had a greater effect on salmon than on the chicken samples. However, roe seem to tolerate up to 18.6 kV/cm and 7 pulses without any visible effect. At the same time, however, the reduction in the number of microorganism was insufficient. This investigation shows that it is not possible to use PEF for treatment of such muscle foods because the voltage level that causes defection in the food is lower than the voltage needed for treatment. As a result, the microstructure of the food is damaged before any treatment can begin.

In conclusion, application of an electric filed of 4 kV/mm and energy of 100 kJ/kg to 200 kJ/kg is effective for liquid food treatment while treating semi-liquid products need higher energy and lower field strength. The PEF method is not applicable for solid foods.

1.3 Power supplies for PEF

In context of the application of PEF, the generation of the desired pulse waveform has always been one of the most challenging tasks. Basically, a charged capacitor delivers energy to the chamber containing the liquid, using a high voltage switch. In most of the research, a decaying impulse waveform has been implemented using thyratrons, ignitrons, or spark gap switches. Matsumoto et al. [34] developd a PEF generator for food treatment using a ceramic capacitor and a rotating spark gap to deliver 20 kV at a repetition rate of 60 Hz. Creyghton et al. [35] connected the output of the spark gap to a pulse transformer in order to obtain a higher voltage. The main disadvantages of such a design are the low repetition rate and the poor controllability of the output waveform. Using an ignitron switch, Washington State University developed a generator that can generate exponential decaying impulses of about 25 kV [36]. This generator has been used by some researchers in PEF applications. References [37, 38, 39] are just some of the examples of the use of decaying impulse waveforms for food treatment applications. However, the energy efficiency of these power supplies is questionable [40]. Moreover, the pulse width and output waveform of the decaying impulse

generators is highly related to the load conductivity and therefore changes according to the temperature [37].

Beveridge et al. [41] used a pulse forming network (PFN) to generate a 30 kV bipolar square waveform. Despite the high efficiency of the square pulses, the repetition rate of the generator is as low as 1 Hz. In addition, the output waveform is dependent on load conductivity, and the PFN should be redesigned for each type of liquid.

Schultheiss et al. [42] implemented a Marx generator with a rating of 300 kV and 40 Hz for treating foods. Because of the low repetition rate of the Marx generator, it is necessary to apply a high level of energy per pulse which may result in damage to the nutritional value of the food.

Novac et al. [43] developed a novel non-invasive method of food treatment. They used an antenna coupled to a high voltage pulsed generator in order to produce an intense pulse electric field. The antenna is covered with a plastic material so that it can be immersed in the liquid. Using this method, it is possible to apply a high electric field with a low current. However, matching the antenna with the load and applying a uniform field are the potential problems associated with this research.

Narsetti et al. [44] used a magnetic compressor to generate voltage as high as 20 kV at 2 kHz. It uses two stages of a compressor circuit and a pulsed transformer to step up the voltage. Fig. 1.3 shows the schematic of this circuit. The generator can generate nanosecond decaying impulse pulses with a peak current of 860 A and an energy of 0.56 J. The main drawback of the generator is the low energy output, the low efficiency of the impulse waveform, and the poor controllability of changing the pulse width.

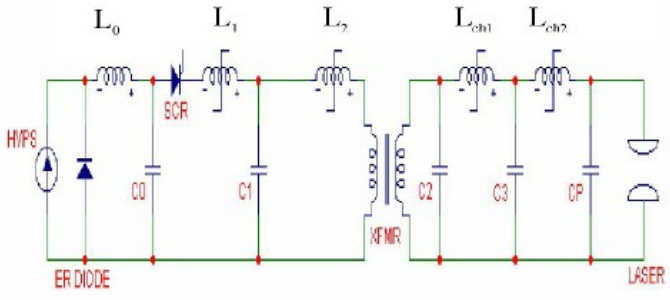

Figure 1.3. Schematic circuit of a magnetic pulse generator [44].

Chang et al. [45] designed and implemented a narrow pulsed generator using a flyback transformer. Their system can generate narrow square pulses up to 5 kV/mm, but the main drawback of their work is the low repetition rate of 6 Hz.

The improvements in semiconductor technology have made it feasible to base the PEF power supply on solid state switches. Semiconductor switches have demonstrated benefits such as high speed switching, highly efficiency, and high controllability. To compensate for the low current and voltage capability of solid state switches, combinations of these switches have been used to produce a high voltage and high current power supply. Grenier et al. [46] used metol oxide field effect transistor (MOSFET) switches in series in order to generate 3 kV square pulses for food treatment. They used small switches, and the results showed that they are suitable for small cuvettes, due to the low voltage and current capability. Tseng et al. [47] also used MOSFET switches to implement a half-bridge series resonant converter in order to generate high voltage. They could produce 10 kV with 5μs pulses at 1 kHz, but the output current is as low as 0.1 A, which is not sufficient for large volume of food.

Insulated gate bipolar transistor (IGBT) switches have a higher voltage blocking capability and also a low on-state voltage. The benefits are the result of the combination of the advantages characteristics of both bipolar transistors and MOSFETs. Zhang et al. [48] used 2200 V, 1200 A IGBT switches in an H-bridge configuration and pulse transformer to deliver 12 kV peak at the output. The maximum output current reported was 720 A peak. The drawbacks of this design are its expensive and complex pulse transformer design and the difficulty of scaling up the system. Fig. 1.4 shows the schematic of their design.

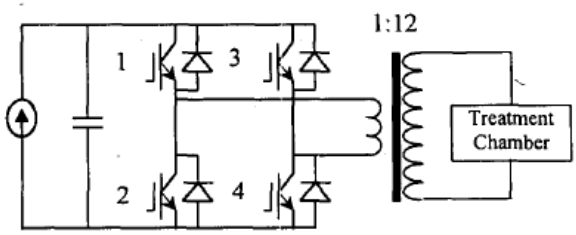

Figure 1.4. PEF generator using an H-bridge and pulse transformer [48].

Beak et al. [49] used the Marx generator principle to implement a high voltage generator. They used IGBT switches as discharging switches, as shown in Fig. 1.5. The maximum output rating is 20 kV, 300 A, and 5 μs at 1 kHz using 16 IGBT modules. The problem with this design is its low speed charging stage and the lack of control, which limits the maximum frequency. With higher levels at the output, the maximum frequency becomes smaller. Ghani et al. [50] also simulated such a design.

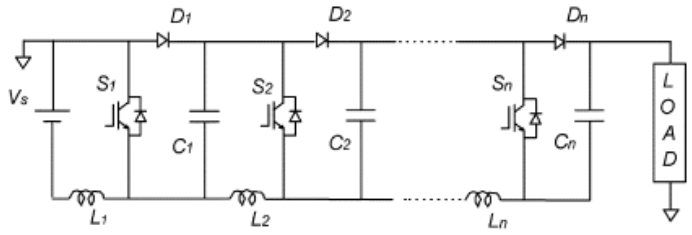

Figure 1.5. Schematic of a solid state Marx generator for food treatment taken from [49].

The research conducted by Gaudreau et al. [51, 52] in this area was particularly valuable. They implemented a commercial PEF unit using IGBT switches and stacked several switches in series to produce a high voltage bipolar pulse generator. Fig. 1.6 shows the schematic of their design. The output of the generator can be as high as 60 kV, 600 A at an average power of 75 kW. They were able to generate square pulses with a fast rise time of about 200 ns at 1 kHz. The drawbacks of their design are the expensive components and the complexity of the design. The 60 kV DC source is difficult and expensive to construct, and because the capacitors must be able to withstand such a voltage, they are also costly. In addition, combining a chain of IGBTs in series adds complexity to the design due to the requirement for a voltage balancing circuit for the series connected IGBTs [53, 54, 55, 56]. Prins et al. [57] also used the same concept to produce a 10 kV generator for food treatment.

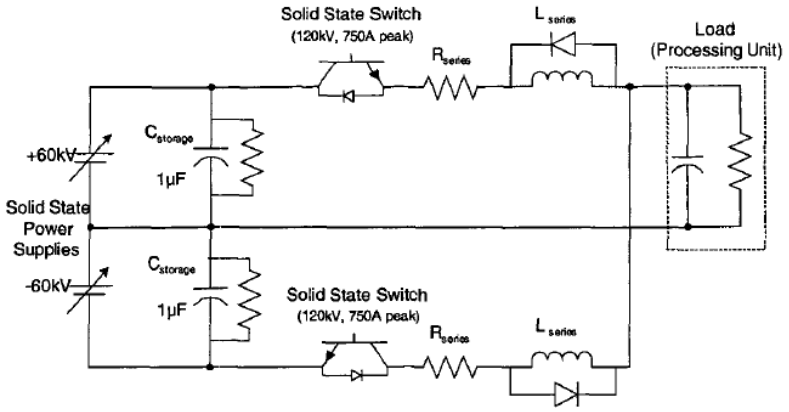

Figure 1.6. Schematic of Diversified Technologies Inc. solid state generator for food treatment [51].

Jayram [58] provided a comprehensive review of generators used in pulsed electric field applications and in the food processing industry which concludes the systems generating square pulses have better performance in compare to the systems with decaying impulse output waveform.

1.4 Motivation

Consideration of the literature review presented in the previous sections, reveals that it is feasible to use the pulsed electric field method as an alternative method of conventional pasteurization and also as an enhancement of extraction processes. Higher quality products can thus be produced using the PEF method. Despite the many systems that have been implemented for treating pumpable food using PEF, few commercially viable solutions are available that can meet all of the needs of the food industry and enable this method to become the dominant pasteurization method. Most of the previously mentioned pulse generators have limited scalability, which results in limited product capacity. Poor treatment efficiency and a high temperature rise in the liquid are the other constraints associated with the previous generators that are based on a decaying exponential waveform. Other common problems in these generators include a limited output frequency that results in small flows of the liquid, complexity of implementation, and their high cost.

The goal of this research is to design and implement a generator that can overcome the abovementioned problems. Using high voltage IGBT switches in a Marx generator topology provides the flexibility needed in order to produce the desired waveform. The voltage and current rating can be adjusted by increasing or decreasing the number of stages or the number of switches. The pulse width and frequency can be easily set through the controller interface panel. Due to the capabilities of the IGBT switches, a high frequency and a high current can be generated at the output, which can result in a high flow rate during the treatment. A square output waveform increases the effectiveness of the treatment, allows the liquid to be treated at a lower temperature, and at the same time, saves energy. Moreover, a voltage multiplier design eliminates the need for a high voltage input DC source, thus reducing the cost of the generator.

1.5 Objectives

The following are the objectives of this research:

- Design and implement a power supply for liquid food treatment applications, based on the Marx generator design and using a combination of 3 kV IGBT switches.
- Demonstrate the possible cascade-ability of the design by implementing the generator in two stages in order to generate 6 kV at the output.
- Implement up to three IGBT switches in parallel in order to increase the current capability.
- Enhance the triggering circuit to achieve faster rise and fall times.

- Implement a variety of types of switches in order to determine the most suitable one for PEF applications.
- Adjust and modify the system in order to perfect the operation of the generator for PEF applications.

In the following chapter, the generator design is discussed, and the trigger unit and digital hardware are explained in Chapters 3 and 4. The results and discussion can be found in Chapter 5, and the conclusions are presented in Chapter 6.

Chapter 2
System Design

The design of the new pulse generator system included the following components: the measurement system, the treatment chamber, the switches, the voltage and current requirements, the voltage waveform, the energy requirement, the circuit design, the design parameters, and the input power stage design.

2.1 Measurement System

A Tektronix 200 MHz, 2Gs (TDS 2024) was used to monitor and analyze the current and voltage waveforms. A Tektronix P6015A high voltage probe with a ratio of 1000:1 was used to measure the voltage. The high frequency current transformers were used to measure the current: an ION PHYSICS CORPORATION CM1L current transformer with a ratio of 0.01 V/A, and a current transformer with a ratio of 0.05 V/A. An FLIR-SC500 infrared camera with thermo-vision acquisition software (ThermaCAM™ Researcher 2.8 Pro) was used to capture the temperature rise in the chamber. The non-contact type of temperature measurement made it possible to continuesly record the temperature changes during the entire pulse treatment. The emissivity was determined by comparing two temperatures: the camera temperature of the sample at 25º C and the temperature as measured using the thermocouple as a reference. A conductivity meter was used to measure the conductivity of the liquids.

2.2 Treatment Chamber

Different types of treatment chambers are used in PEF applications: needle-plate, plate-plate and pipe type. For this project a specially designed chamber shown in Fig. 2.1 was used. The design which has been patented by the University of Waterloo [59], allows the liquid to flow from the center of the inner stainless steel electrode through a 1.27 mm gap between two electrodes. Voltage applied to the electrodes produces a uniform electric field across the liquid to be treated. Although the test set up can be used for a continuous flow, only batch mode test results are presented in this study. This option allows the quantification of the temperature rise in a 2D pattern using IR camera.

Figure 2.1. Treatment chamber showing the electrode spacing and the uniformity of the treatment zone.

2.3 Switches

In PEF technology, the charging voltages of the power supplies are generally 1 kV/mm to 6 kV/mm, while current depends on the conductivity of the liquid and the design of the treatment chambers. Several types of switches are capable of generating the desired voltage and current that are used in PEF systems, including spark gaps, trigatrons, ignitrons, thyratrons, and semiconductors. Spark gap switches can hold ~100 kV and can withstand very high currents in the order of MA. They are used in Marx generators but can be fired only at rates of 1Hz to 100 Hz which is too low. Trigatron is a controlled spark gap switch which includes a trigger unit that produces a controlled small spark, initiating the arc over the main gap. As with the spark gap switches the low speed of the switching is a problem. Ignitron, which is a type of controlled rectifier, has a high current capability but is not frequently used in PEF systems due to improper handling and triggering. Thyratron is a gas-filled discharge chamber with a cathode, one or several grids, and an anode. Its operating voltage range is up to ~100 kV at ~10 kA and 5 kHz to 10 kHz. This switch is widely used in PEF. However, it requires a complex driver circuit, making it one of the most expensive switching devices. All of the above switches are opening or closing switches and cannot produce a square waveform. A pulse forming network (PFN) is therefore required with these switches, which is difficult to implement. Solid state switches provide better performance, are easier to handle, require fewer components, allow faster switching times compared to older power switches, and are more economically priced. Fig. 2.2 shows the range of operation for each type of solid state switch.

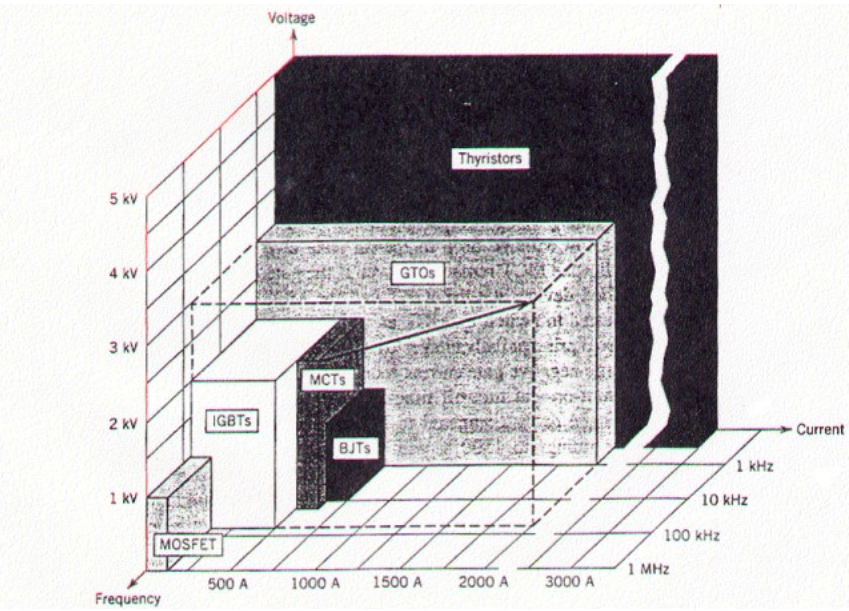

Figure 2.2. Voltages, currents, and frequency capabilities of different types of power electronics semiconductor switches [60].

One of the first developed switches in this group is the gate turn-off (GTO) thyristor. This switch has relatively low efficient switch. A second type, bipolar transistors, also produces high power dissipation and low efficiency. Neither of these types of switches is used in PEF applications. A Metal-oxide semiconductor field-effect transistor (MOSFET) is a high frequency switch widely used in electronics, but because of high on-state resistance, they are not suitable for PEF applications. Insulated-gate bipolar transistors (IGBT) combine the best features of MOSFET input and bipolar transistor output in a newer power-switching device. Its advantages are very rapid switching and small power consumption. The only disadvantage of these switches is a voltage switching limit ~4 kV, thus requiring a series connection to produce high voltages. Based on these considerations, for PEF applications, the best choice among the solid state switches is the IGBT. Its reasonable price made it feasible to use several IGBTs as a series chain to overcome the low voltage capability or to connect them in parallel to increase the current. Accordingly, the following switches were selected:

- IXBX55N300 manufactured by the IXYS Company, rated for 3 kV and 55 A (Fig. 2.3); the switch is built using BIMOSFET technology which provides a positive temperature coefficient.

- CM600HA-24A manufactured by the Powerex Company, rated for 1.2 kV and 600 A (Fig.2.4); the switch parameters are listed in Table 2.3.1.

High Voltage, High Gain BiMOSFET™

Monolithic Bipolar MOS Transistor

IXBK55N300
IXBX55N300

V_{CES} = 3000V
I_{C110} = 55A
$V_{CE(sat)}$ ≤ 3.2V

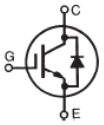

TO-264 (IXBK)

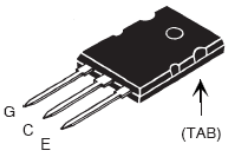

PLUS247™ (IXBX)

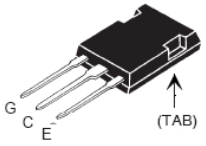

G = Gate C = Collector
E = Emitter TAB = Collector

Symbol	Test Conditions	Maximum Ratings	
V_{CES}	T_J = 25°C to 150°C	3000	V
V_{CGR}	T_J = 25°C to 150°C, R_{GE} = 1MΩ	3000	V
V_{GES}	Continuous	±25	V
V_{GEM}	Transient	±35	V
I_{C25}	T_C = 25°C (Chip Capability)	130	A
I_{LRMS}	T_C = 25°C (Lead RMS Limit)	120	A
I_{C110}	T_C = 110°C	55	A
I_{CM}	T_C = 25°C, 1ms	430	A
SSOA (RBSOA)	V_{GE} = 15V, T_{VJ} = 125°C, R_G = 2Ω Clamped Inductive Load	I_{CM} = 110 @0.8 • V_{CES}	A
T_{SC} (SCSOA)	V_{GE} = 15V, T_J = 125°C, R_G = 10Ω, V_{CE} = 1250V, Non-Repetitive	10	µs

Figure 2.3. IXBX55N300 specifications [61].

Figure 2.4. CM600HA-24A package [62].

Table 2.1. CM600HA-24A specifications [62].

Ratings	Symbol	CM600HA-24A	Units
Junction Temperature	T_j	–40 to 150	°C
Storage Temperature	T_{stg}	–40 to 125	°C
Collector-Emitter Voltage (G-E Short)	V_{CES}	1200	Volts
Gate-Emitter Voltage (C-E Short)	V_{GES}	±20	Volts
Collector Current (DC, T_C = 87°C)*4	I_C	600	Amperes
Peak Collector Current (Pulse, Repetitive)*2	I_{CM}	1200	Amperes
Maximum Collector Dissipation (T_C = 25°C)*2,*4	P_C	3670	Watts
Emitter Current (T_C = 25°C)	I_E*1	600	Amperes
Peak Emitter Current (Pulse, Repetitive)*2	I_{EM}*1	1200	Amperes
Mounting Torque, M6 Main Terminal	—	26	in-lb
Mounting Torque, M6 Mounting	—	26	in-lb
Mounting Torque, M4 G(E) Terminal	—	13	in-lb
Weight	—	480	Grams
Isolation Voltage (Main Terminal to Baseplate, f = 60Hz, AC 1 min.)	V_{ISO}	2500	Volts

2.4 Voltage Requirements

As mentioned in the literature, to produce non-reversible breakdown and to kill the bacteria requires that an electric field higher than a specific threshold be applied across the living cell for a fixed amount of time, in the order of microseconds [1]. The electric field applied breaks the cell membrane by expanding the pore and causing the death of the cell. It must induce voltages across the cell's membranes that are greater than the critical trans-membrane potential of 1 V. Assuming the application of the field in the direction of the cell's membrane, as shown in Fig. 2.5, and a radius of 0.04 μm for the membrane, the minimum level of the electric field for successful inactivation using (2.4.1) can be calculated as 16 kV/cm, as follows:

$$V=1.5\ r\ E\cos\theta \qquad (2.4.1)$$

where *r* is the radius of the cell, E is the electric field and θ is the angle between the electric field and the membrane, which is assumed to be zero.

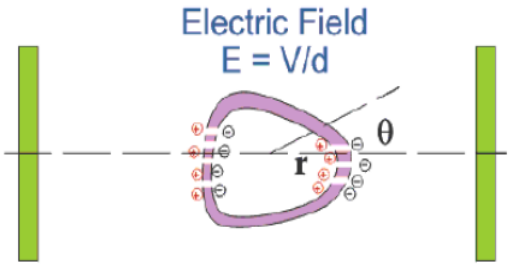

Figure 2.5. Living cell under application of electric field [63].

In the studies reported in the literature, the amount of the field applied for successful inactivation in PEF applications varied from 1 kV/mm to 6 kV/mm. However, the lower field levels were used in extraction processes. Considering the test conditions and the results observed in the literature, a field level of 4 kV/mm seemed to be a suitable value to use as the electric field selected for this research.

The level of the field strength and the gap design dictates the required voltage level at the output of the generator. Using a gap size of 1.27 mm, a voltage level of 5.1 kV would have to be generated and delivered to the chamber.

2.5 Current Requirements

Although the electric field is the parameter that causes inactivation, the current required for the treatment must also be supplied. A current associated with the conductivity of the liquid passes

through the chamber at the field applied, thus delivering energy to the liquid. Treatment chamber can be modeled as resistive load parallel with a capacitance. Because the resistance of liquid foods, in a selected chamber, is very small compared to their capacitance, the load can be taken as purely resistive. Table 2.2 shows the measured conductivity of a variety of liquid foods and their resistance values in the test chamber.

Table 2.2. Conductivity of liquid foods and their equivalent resistance in the treatment chamber with 1.27 mm gap.

Type of Liquid	Conductivity (μS/cm)	Equivalent Resistance in the Test Chamber (Ω)
Tap Water	700	12.5
Apple Cider	1000	10
Apple Juice	1700	8
Orange Juice	2400	5.1
Tomato Juice	15000	0.65

As can be seen, the amount of current depends on the liquid conductivity as well as the chamber size and geometry, which can be varied from several hundred to several thousand amperes in practice. IGBT switches should therefore have both a high peak current rating and the capability of working in parallel. Despite the high current requirement, the actual steady state current rating of the switch can be much smaller due to the short pulse width of the waveform. In this study, 3 kV IGBTs manufactured by IXYS using BIOMOSTEF technology were implemented. Their rated current is 55 A, but they can conduct an 800 A peak current under a pulsed condition. Their positive temperature coefficient makes these switches capable of being connected in parallel. This characteristic causes the conducting resistance to rise in the switch when it is subjected to higher current, compared to other types of switches. The increased current is thus reduced automatically and balances the current in the switches. Therefore, increasing the number of switches in parallel makes it possible to increase the output current to the desired level.

2.6 Voltage Waveform

One of the most important parameters in the PEF process is the voltage waveform. As it mentioned, only the part of the voltage applied with the field higher than the threshold will result in killing the

microorganisms; the rest of the voltage applied causes energy to be wasted as heat in the liquid, which not only diminishes the energy efficiency but also raises the temperature in the liquid. In Fig. 2.6, the shaded area represents the part of the electric field that is below the threshold E_{th} and that results in a rise in temperature without any inactivation. Because the PEF process is non-thermal, a rise in temperature has adverse effect and requires a heavier cooling system. Temperatures higher than 40º C can affect the taste and nutrition of the liquid and temperatures higher than 60º C causes the initiation of the pasteurization process [9]. Square waves are thus strongly preferred over exponential decaying impulses. Square pulses with a short duration and fast turn-on and turn-off times are the most efficient because the process can be optimized to result in a minimal rise in the temperature of the liquid. It has also been reported that a flat top square pulse is more effective for inactivation than exponential decay pulses with similar energy per pulse [64, 40].

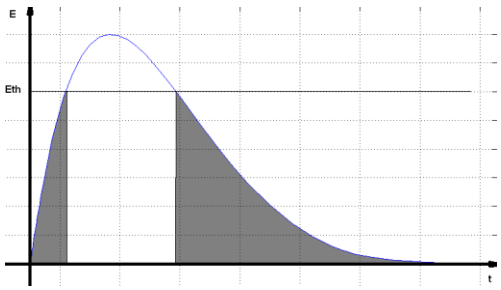

Figure 2.6. Energy dissipation in a decaying impulse waveform.

2.7 Energy Requirements

The energy applied per unit of volume is one of the most important parameters in the PEF process. Applying more energy than required causes the temperature to rise which initiates thermal treatment and affects the nutrition of the liquid as well as reducing the energy efficiency of the system. On the other hand, an energy level that is too low may result in an ineffective process. Selecting appropriate level is therefore critical. Despite the fact that the energy levels reported in the literature for PEF vary from 100 kJ/kg to 1000 kJ/kg [65], applying 100 kJ/kg to 200 kJ/kg seems more reasonable for liquids whose conductivity is about 1000 µS/cm to 3000 µS/cm. However, the application of higher energy levels has been reported for solid-liquid and extraction applications. The total energy of the system can be determined using the energy applied per unit of volume and the flow rate of the liquid. For example, for applied energy of 150 J/mL and a flow rate of 100 mL/s, total energy of 15000 J/s is required. The repetition rate of the pulses can be determined using the energy value and the size of the chamber.

2.8 Circuit Design

The developed design uses a Marx generator configuration in which the capacitors are charged in parallel and are discharged in series. Fig. 2.7 shows a simplified schematic of the design for multiple stages. The benefits of this design include cascade-ability, a smaller DC input voltage, and simple snubber circuits to balance the switches connected in series.

Capacitors C1 and C2, shown in Fig. 2.8 are charged in parallel through diodes D1 and D2 when charging switches SW1 and SW2 are ON. Fig. 2.9 shows the equivalent circuit during the charge process. The charging time can be quite slow compared to the discharging time. The charging current can therefore be reduced in order to minimize the current rating of the switch.

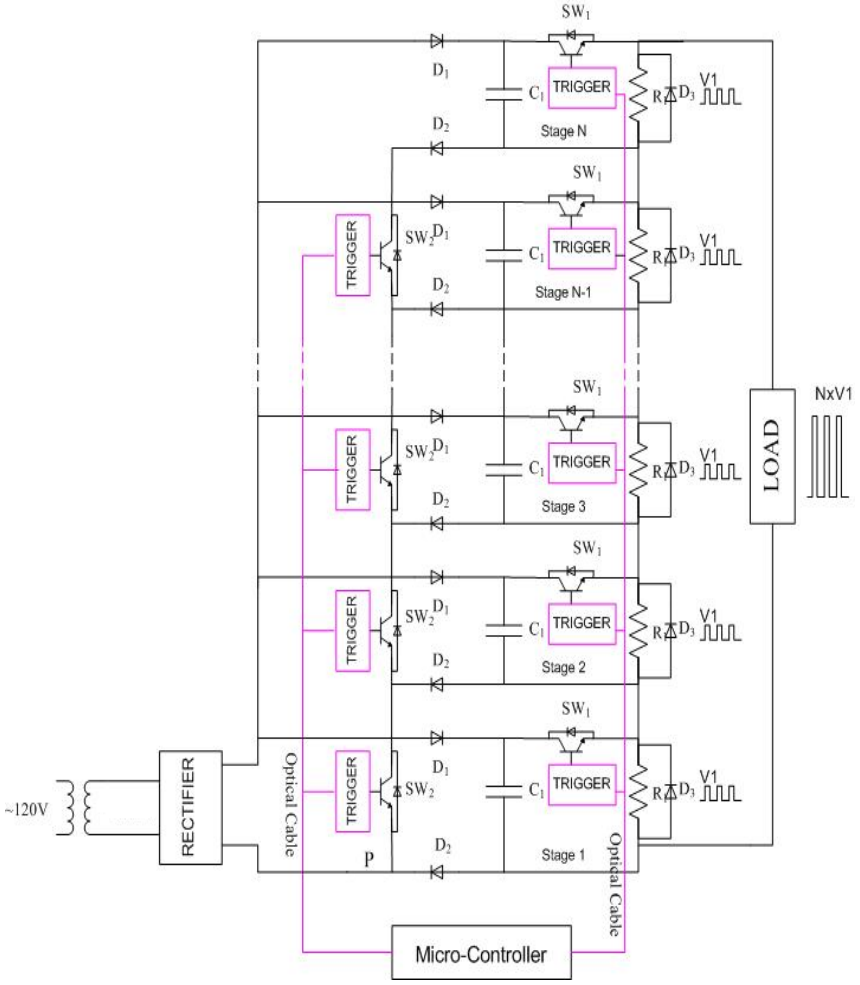

Figure 2.7. Generator schematic [66].

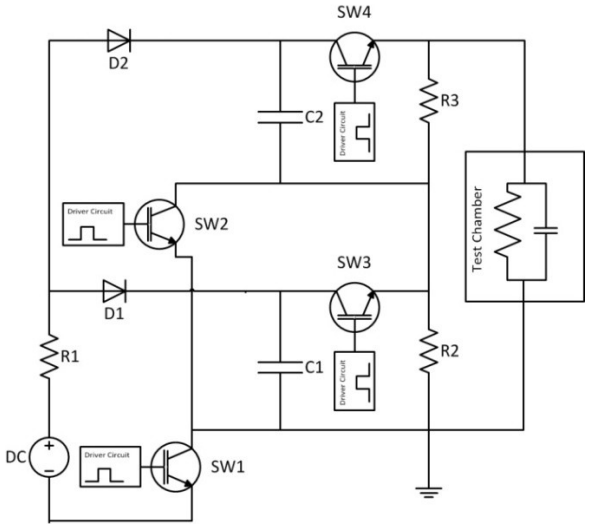

Figure 2.8. Schematic of a solid state Marx generator.

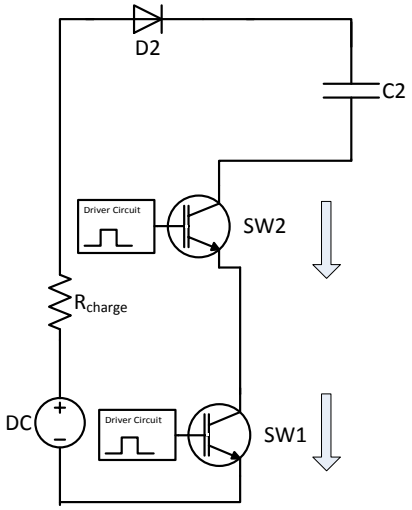

Figure 2.9. Equivalent circuit of the charging cycle.

As the capacitors are charged, the charging switches are turned off, and after a dead time, the discharging switches (SW3 and SW4) are turned on. The capacitors connected in series, thus deliver twice the maximum DC charging voltage to the load. Fig. 2.10 shows the equivalent circuit for the discharge process. The dead time should be adjusted in such a way that a good interlock is provided between the charging and discharging switches. If both switches turn on at the same time, the short current path will burn out the switches. Resistors R2 and R3 are used to discharge the capacitor charge when no load is connected to the output. These resistance values should be several kilo ohms in order to prevent adverse effect on functionality during normal generator operation. D3 and D4 make an alternative current pass for the circulation of current of stray inductances.

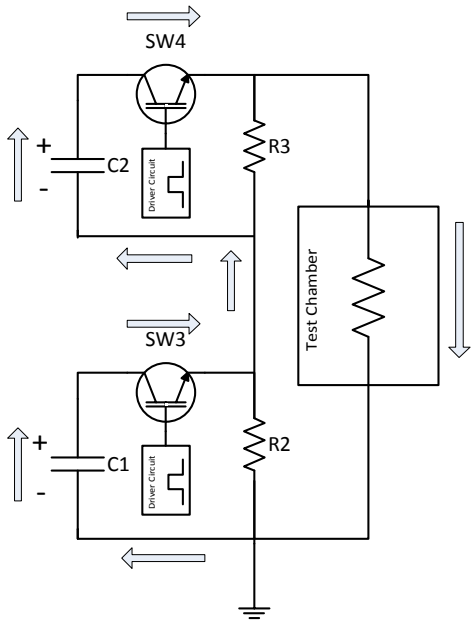

Figure 2.10. Equivalent circuit of the discharging cycle.

The pulse width is adjustable through the controller and can be varied from 1 μs to 10 μs. Greater pulse widths can be generated but are not practical for PEF applications. The DC bus is adjustable between 0 kV and 3 kV; therefore, a maximum peak voltage of 6 kV can be generated at the output terminal, using two stages. The design allows a multi-stage set up, with a large number of stages in order to generate high amplitude pulses. A relatively low current, high voltage pulse generator with ten stages has been built and implemented for testing insulation strength [66]. A photograph of the complete system used in this study is presented in Fig. 2.11.

The current ratings of the discharging switches should be as high as possible; a higher current capability makes it possible to treat liquids with higher conductivity or to increase the gap size in order to achieve a higher flow rate. The discharging switches are 3 kV, 55 A IXYS IGBTs (IXBX55N300), but they can conduct an 800 A peak current under pulsed conditions. To deliver more current to the load, the IGBTs can be connected in parallel at each stage. The existing generator with two stages and two switches in parallel at each stage is capable of generating 6 kV and 1.6 kA at the output terminals, depending upon the load.

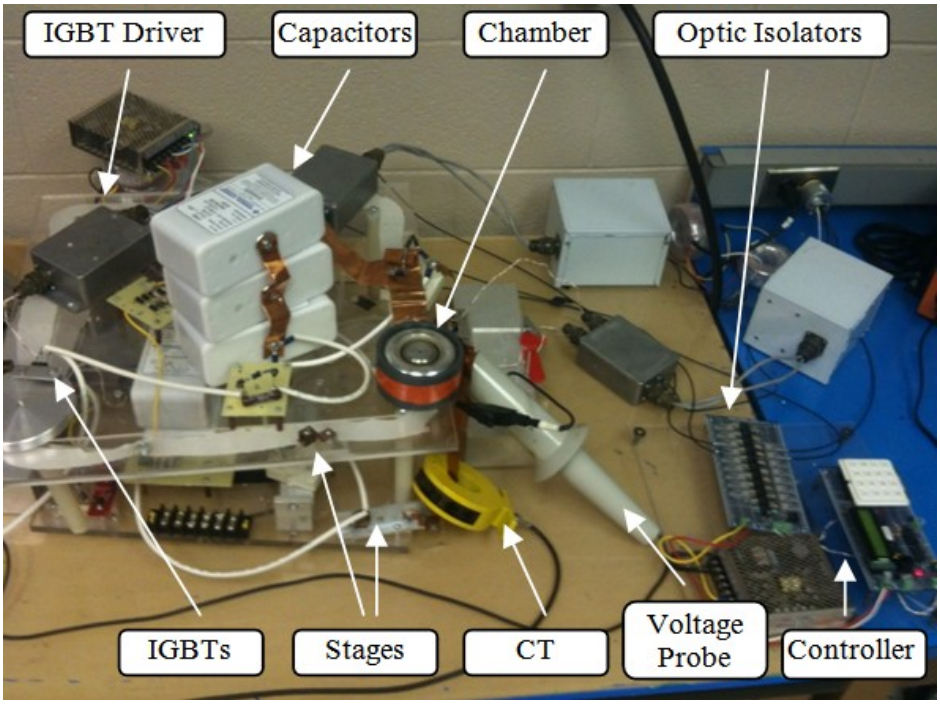

Figure 2.11. Test setup with two stages and two switches in parallel in each stage.

2.9 Design Parameters

Because all parameters are related to one another so that changing one parameter can affect the others, it was necessary to calculate all of the parameters with respect to the others. The parameters are also dependent on the capabilities of the generator. The assumptions used in the design of the system are listed in Table 2.3.

Table 2.3. The design parameters.

Parameter	Rating
Electric field applied	40 kV/cm
Energy per unit of volume	150 J/mL
Chamber volume	66 mL
Chamber gap size	1.27 mm
Maximum liquid conductivity	3300 µS/cm
Maximum flow rate	100 mL/s
Pulse width	2-5 µs

The calculation of the design parameter was based on the assumptions listed in Table 2.3. The maximum output voltage was calculated as follows:

$Vout_{max} = E \times Chamber\ gap\ size = 4 \times 1.27 = 5.08\ kV$ (2.9.1)

where $Vout_{max}$ is the maximum output voltage, and E is the field applied. To achieve this level of the voltage required two stages of the generator. With a maximum conductivity of 3300 µS/cm and using Eq. (2.9.1) and Table 2.2, the minimum resistance as the load (R_{min}) for the existing chamber was determined to be 5.1 Ω. The maximum current ($Iout_{max}$) could then be calculated as:

$$Iout_{max} = \frac{Vout_{max}}{R_{min}} = \frac{5.08\ kV}{5.1\ \Omega} \cong 1kA \quad (2.9.2)$$

Assuming an 800 A peak current for each switch, two switches in parallel were needed to handle this current.

Once the maximum output voltage, current, and pulse width were calculated and assuming the output waveform to be square, the energy per pulse was found approximately:

$$Energy\ per\ pulse \cong Vout_{max} Iout_{max}\ PW \cong 5.08\ kV \times 1kA \times 2\mu s = 10\ J\ /pulse \quad (2.9.3)$$

In the next step, the total energy and maximum frequency were calculated, as follows:

$Total\ Energy\ per\ second = Energy\ per\ unit\ of\ volume \times Max\ flow\ rate = 15000J/s$ (2.9.4)

$$Frequncy = \frac{Total\ Energy\ per\ second}{Energy\ per\ pulse} = 1.5\ kHz \quad (2.9.5)$$

Using the results of Eq. (2.9.3) and (2.9.1), it was possible to calculate the total capacitance value:

$$Energy\ per\ pulse = \frac{1}{2}\ C\ Vout_{max}^2 \rightarrow 10 = \frac{1}{2}\ C\ (5.08\ kV)^2 \rightarrow C = 0.78\ \mu F \quad (2.9.6)$$

Considering a safety margin, the total capacitance was taken to be 1 µF. The capacitance of each stage was thus 2 µF, which resulted in a total capacitance of 1 µF within 2 stages because they form a series connection during discharge cycle. It should be noted that these capacitors must be able to withstand the entire input voltage of 3 kV. The voltage rating of these capacitors is therefore 5kV, including a safety margin. The series inductance of these capacitors is also important and should be as low as possible. The capacitor selected is designed for pulse applications and has a series inductance of 0.016µH.

Having a maximum 1.5 kHz pulse frequency and neglecting the discharge time, results 666 µs for the capacitor to be fully charged. On the other hand, the maximum peak current is drawn from the

switch when the capacitor is fully discharged. The charging resistance was thus calculated to be 133.2 Ω using the following equation and was taken as 100 Ω for simplification.

$$\tau \cong 5R_{charge} \times C \rightarrow R_{charge} = \frac{\tau}{5C} = \frac{666 \times 10^{-6}}{5 \times 1 \times 10^{-6}} = 133.2\ \Omega \quad (2.9.7)$$

The maximum peak current was then determined as follows:

$$I_{peak} = \frac{V_{in}}{R_{charge}} = \frac{3000}{100} = 30A \quad (2.9.8)$$

A charging switch that can carry a 30 A peak current for a short time was required. IXBH12N300 from IXYS Company was selected as the charging switch. Despite the low current rating of 12 A, it is capable of providing the desired current under the pulse conditions while also having a relatively low price.

The diodes must be able to withstand the whole DC voltage (3 kV). They were constructed by using several diodes in series to make a diode chain, which also required an equalizing resistor in the order of 100 kΩ in parallel with each diode in order to prevent overvoltage.

2.10 DC input voltage stage

As mentioned, to generate the threshold electric field for membrane breakdown, for the condition set with the treatment chamber a minimum voltage of 5 kV is required. Hence, the DC voltage should be 3 kV in order to deliver the maximum 6 kV using two stages. This voltage was generated by the circuit shown in Fig. 2.12. A voltage of 110 V AC is fed into a transformer to produce voltage of 3 kV AC, and after rectifying, the DC voltage appears on the output. A schematic of the input stage is shown in Fig. 2.12.

To regulate the input DC voltage, a capacitor had to be installed at the output terminal of the transformer. The capacitance of this element was calculated based on the energy and ripple requirements. In the worst case scenario, this capacitor should supply the entire circuit for half the period of sinusoidal input (assuming that the charging duration of the capacitor is negligible). As a result, it should supply the circuit while the voltage is in the allowable range. The DC voltage ripple was assumed to be ±10 % maximum. This level was forced because of the available high voltage capacitor. It should be noted that a larger capacitor should be implemented to reduce THD level.

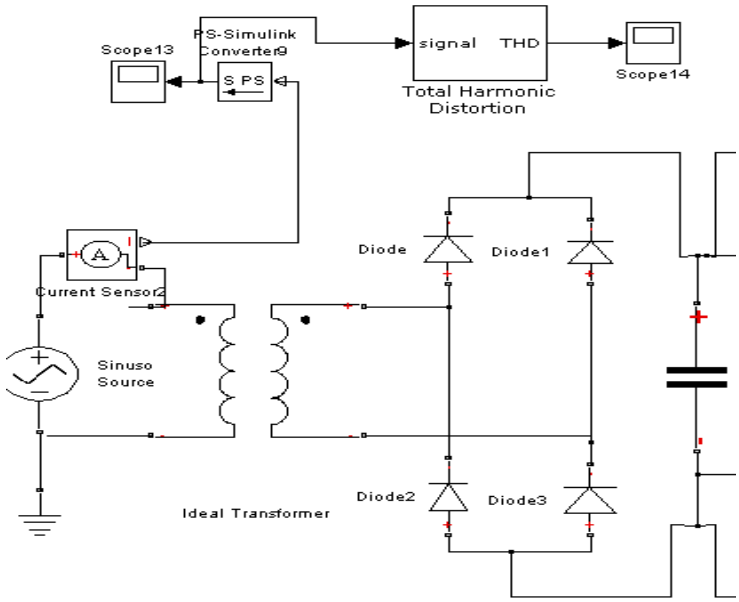

Figure 2.12. Input stage circuit including the AC input and rectifier for generation of input DC high voltage.

The energy to be supplied by the capacitor was calculated as follows:

$$E_{charge} = Energy\ per\ second\ \times half\ period = 15\frac{kJ}{s} \times \frac{1}{120}s = 125\,J \qquad (2.10.1)$$

On the other hand, the energy is also equal to:

$$E_{charge} = \frac{1}{2}\,C_{in}\,(V_1^2 - V_2^2) \qquad (2.10.2)$$

where $V_1 = 3300$ and $V_2 = 2700$. Finally C_{in} was determined to be 70 µF. The voltage rating of this capacitor was then required to be at least 4 kV.

The design requires an input transformer with a voltage rating of 110/3000 V. In this case, the maximum voltage of the DC bus would then be 4240 V, which can be adjusted using an regulated transformer at the input side. The power rating was determined based on the energy consumption which was 15k J/s. Therefore, incorporating a safety factor and considering the reactive power, a power level of 20 kVA was selected. Another important point which should be mentioned here relates to input current, which, because of the pulsed nature of the converter, it is expected to have poor THD and an input filter is required.

Chapter 3
Trigger Unit Design

This chapter explains the design and functioning of the trigger unit including the driver ICs, the circuit design, and its power supply.

3.1 Introduction

The waveform generated using the controller should be employed to drive the IGBT. The output signal of the controller should hence be converted to strong pulses with a suitable voltage and current amplitude to drive the gate of the IGBTs. Moreover, the drive pulses must be resistant and robust with respect to the noise that occurs during the severe switching conditions that result from the high voltage and high current of the IGBT switches. Fig. 3.1 shows a block diagram of the trigger unit for two stages. Designing a suitable drive circuit is thus a challenging task which is discussed in the following sections.

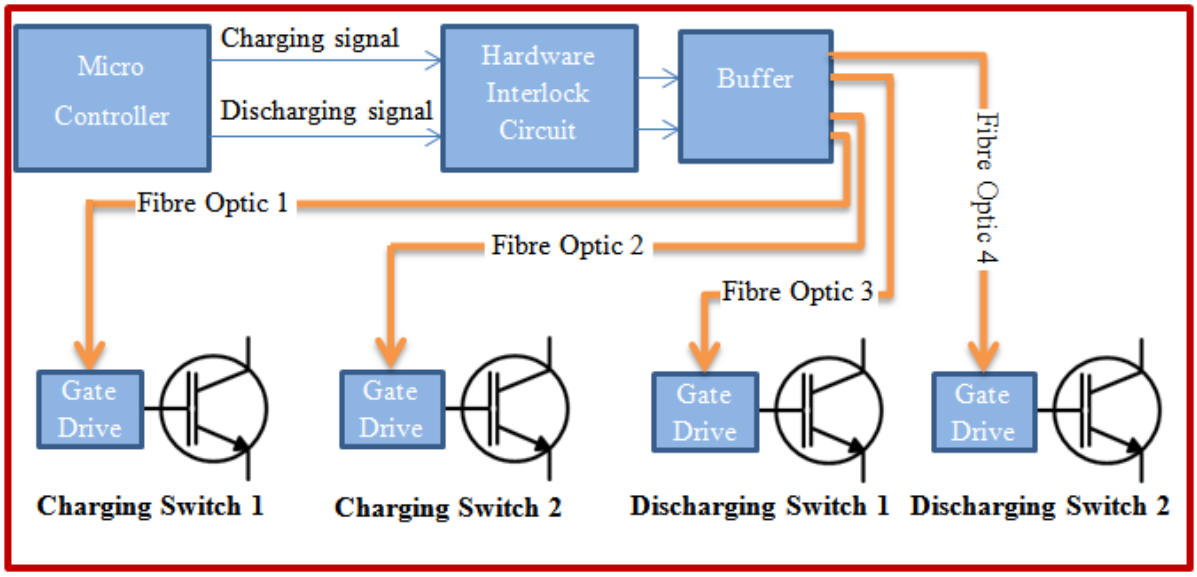

Figure 3.1 Block diagram of the triggering system.

The charging and discharging signal are complementary with a dead time on both sides of the discharging state. To ensure that these signals never activate at the same time in the case of controller failure or other unexpected problems, a simple interlock circuit was implemented for the charging and

discharging signals. Fig. 3.2 shows the schematic of the interlock. A 7408 IC was used as the AND gate and 7404 IC is used as the NOT gate.

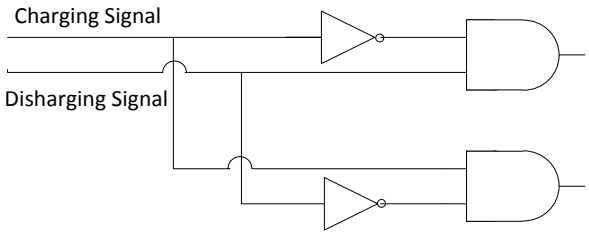

Figure 3.2. Schematic of the interlock block.

The output of the controller is a 0 V or 5 V digital signal and should be buffered to drive the optical transmitters. An optical transmitter and receiver were used to isolate the controller from the gate drive circuit with respect to any electrical connection. Using an optical fibre make it possible to connect the drive circuit to the high voltage nodes of higher stages. It also helps prevent the propagation of any electric noise from the power side to the controller and enables the controller to be installed far from the power circuit. This feature enhances the protection of the circuit from electromagnetic interference (EMI). The electric signal at the transmitter is converted to an optical signal and propagates through the fibre optic cable to the receiver where it would be converted to an electric signal again, to be used for the drive circuit. This optical connection has a maximum signal rate of 5 MBd. Fig. 3.3 shows the schematic of the optical transmitter and receiver. The signal received from the optic isolator is buffered using a TLP250 chip and can be fed into the IGBT gate drive chip.

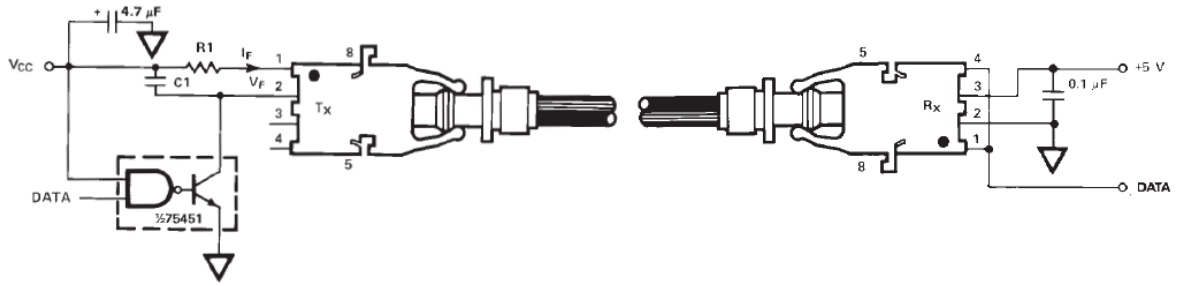

Figure 3.3. Fiber optic transmitter and receiver.

3.2 IGBT Driver ICs

An IGBT can be driven by many circuits and ICs. However, due to the special pulsed application, selecting a suitable chip was challenging. To obtain maximum performance, several driver chips were tested, including the TD351, TC4421, and MIC4451. Table 3.1 provides a comparison of the driver chip parameters, and the next sections describe in greater details.

Table 3.1. A comparison on the various parameters of the driver chips.

Chip Name	Maximum Output Current	Maximum Supply Voltage	Rise Time
TD351	1.3 A	28 V	100 ns
TC4421	9 A	20 V	28-34 ns
MIC4451	12 A	20 V	20-40 ns

3.2.1 TD351 Driver Chip

The TD351 is manufactured by STMicroelectronics. It can provide a drive current of up to 1.3A [67]. Fig. 3.4 shows the detailed internal schematic of the TD351 and its external required components. The input of the TD351 is compatible with both the optical-couplers and the pulse transformers. The input voltage is internally clamped at about 5 V to 7 V. The gate on-state voltage level is +12V, and the gate off-state voltage level is -5 V, with a gate resistance of 15 Ω. Thus, the approximate maximum drive current is *(12+5)/15 = 1.13 A*, which is in the operating current range of the TD351.

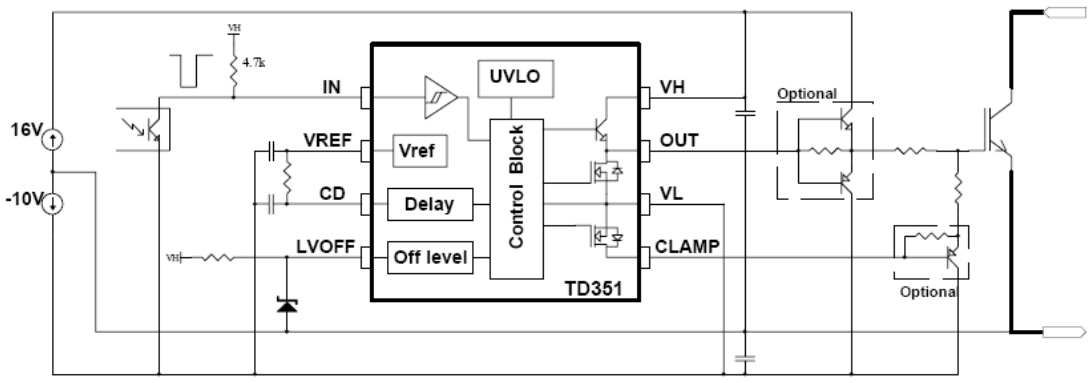

Figure 3.4. Typical schematic and internal block diagram of the TD351 driver chip [67].

The main problems with this chip are the need to have a negative source and the low output current capability. This chip is suitable for high current switches such as the charging switches but it is not appropriate for low current switches.

3.2.2 TC4421 Driver Chip

The TC4421 is manufactured by the Microchip Company and is designed for a high current and high speed switching. The maximum output current can be as high as 9 A, and the supply voltage can range between 4.5 V and 18 V [68]. The chip has latch up protection for up to 1.5 A reverse current. The internal block diagram of the chip is shown in Fig. 3.5.

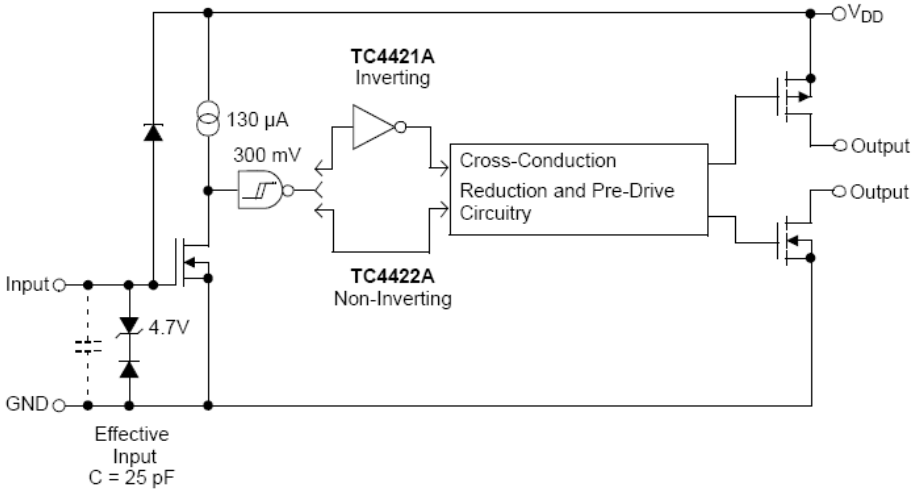

Figure 3.5. Block diagram of the TC4421 driver chip [68].

3.2.3 MIC4451 Driver Chip

The MIC4451 chip is manufactured by the Micrel Company. The features of this chip include having latch up proof, matched rise and fall times of 25 ns, and a high capacitive load drive of 62000 pF [69]. Its power supply operating range is between 4.5 V and 18 V. The most important capability of this chip is its high output current of 12A. The internal block diagram is shown in Fig. 3.6.

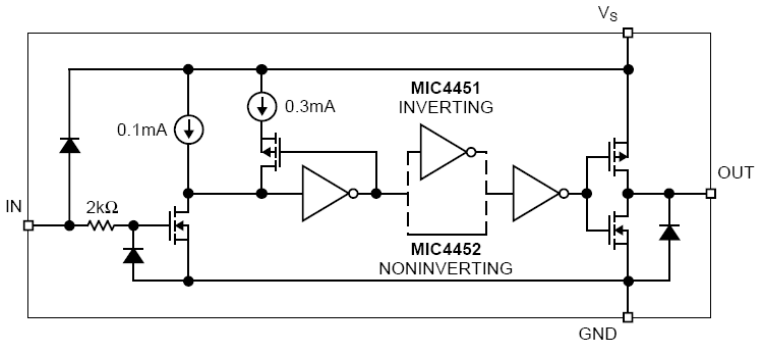

Figure 3.6. Internal block diagram of the MIC4451 driver chip [69].

3.3 Trigger Circuit Design

To successfully drive an IGBT, it is important to know its characteristics with respect to driving the gate. Fig. 3.7 shows a typical model of an IGBT.

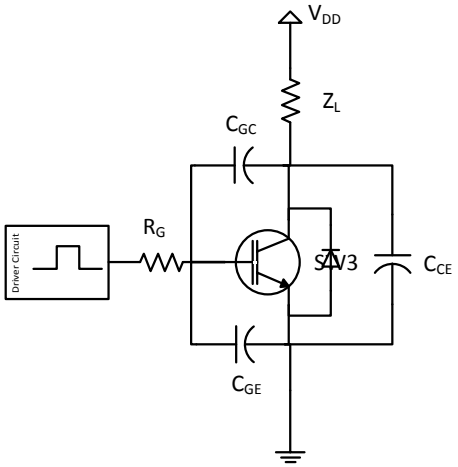

Figure 3.7. IGBT model showing input, output, and reverse transfer capacitances; C_{GE} = gate emitter capacitance, C_{GC} = gate collector capacitance and C_{CE} = collector emitter capacitance.

Input and output capacitances are usually provided in the switch data sheet. Table 3.2 shows a part of IGBT datasheet.

Table 3.2. Input, output, and reverse transfer capacitance of IXBX55N300; Cies = input capacitance, i.e. Cies= CGS + CGC , output capacitance Coes= CGC + CCE ; and reverse transfer capacitance Cres= CGC [61].

C_{ies}	V_{CE} = 25V, V_{GE} = 0V, f = 1MHz	7300	pF
C_{oes}		275	pF
C_{res}		83	pF

These capacitances belong to dynamic characteristics of the switch and change with the collector emitter voltage (V_{CE}). Fig. 3.8 shows the variations in the dynamic capacitances in term of V_{CE}.

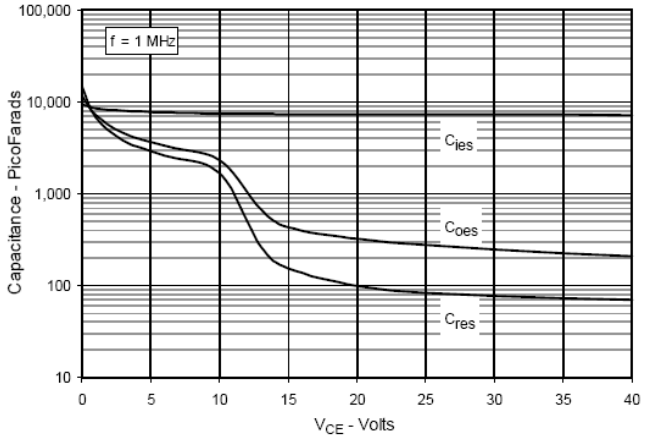

Figure 3.8. The variations in the dynamic capacitances relative to the V_{CE} [61].

Turning on the IGBT requires that the gate charge requirement of the switch, which is related to the abovementioned capacitances, be fulfilled. The total gate charge of Q_G is the amount of charge needed for the switch to be turned on. It can be represented as follows:

$$Q_G = Q_{GE} + Q_{GC} + Q_{OD}$$

where Q_{GE} is the gate to emitter charge, Q_{GC} is the gate to collector charge (miller charge), and Q_{OD} is the override charge after the miller capacitance is charged. Fig. 3.9 shows the above relationship. As can be seen, the gate voltage should be much higher than the threshold voltage in order to have a strong turn on [70].

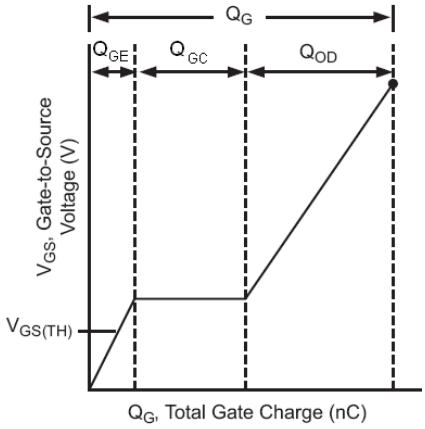

Figure 3.9. The variation of the gate-source voltage relative to the total gate charge Q_G [70].

Fig. 3.10 shows the real curve of the gate charge relative to the gate-emitter voltage from the datasheet of the IGBT for IXBX55N300. As can be seen at the highest value of V_{GE} , the gate charge Q_G is about 335 nC. This value was measured under specific test conditions and it can be higher with higher voltages.

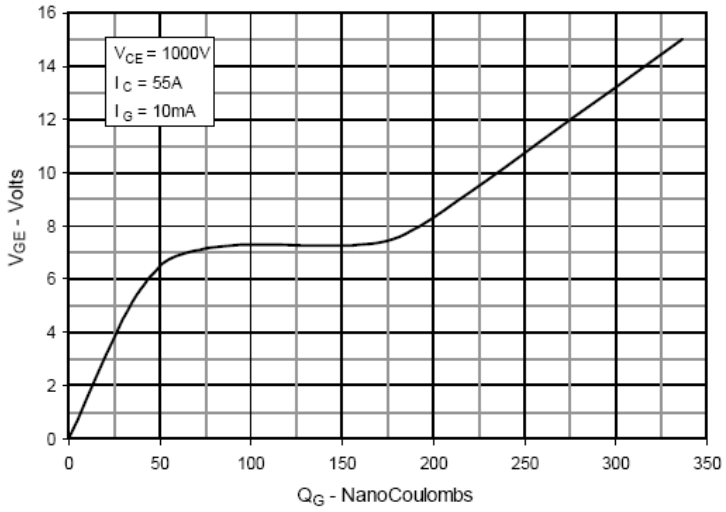

Figure 3.10. V_{GE} - Q_G curve of the IXBX55N300 [61].

For a gate charge of 335 nC and assuming a rise time of 100 ns for the switch, the maximum peak current needed at the output of the gate drive was calculated using following formula:

$$I_G = \frac{Q_G}{t_{transition}} \tag{3.3.1}$$

$$\rightarrow I_G = \frac{335\ nC}{100\ ns} = 3.35\ A$$

This value can be higher because of the higher gate voltage. Obviously, the TD351 has a smaller output current capability and cannot be used for the discharging switches. Both the TC4421 and MIC4451 can generate such a current.

The performance of the driver chips was tested for different switches. For this test, liquid with two different conductivities were selected as the load: 500 µS/cm and 1000µS/cm. Two type of switches, namely, IXBX55N300 (3kV, 55A) and CM600HA-24A (1.2kV, 600A) were tested using two driver ICs: TC4421 (9A) and MIC4451 (12). The rise and fall times of the output voltage for one stage and one switch configuration of the generator were recorded. The results are shown in Table 3.3.

Table 3.3. Comparison of the rise and fall times of two switches with respect to the driver circuit current under different conductivities.

		IXBX55N300		CM600HA-24A	
		Rise Time	Fall Time	Rise Time	Fall Time
1000 µS/cm	9 A	412 ns	200 ns	274 ns	386 ns
	12 A	395 ns	191 ns	255 ns	420 ns
500 µS/cm	9 A	210 ns	154 ns	130 ns	800 ns
	12 A	184	155 ns	125 ns	820 ns

Fig. 3.11 shows the gate voltage and current of the IXBX55N300 (left) and the CM600HA-24A (right) driven by the MC4451 (12 A) chip.

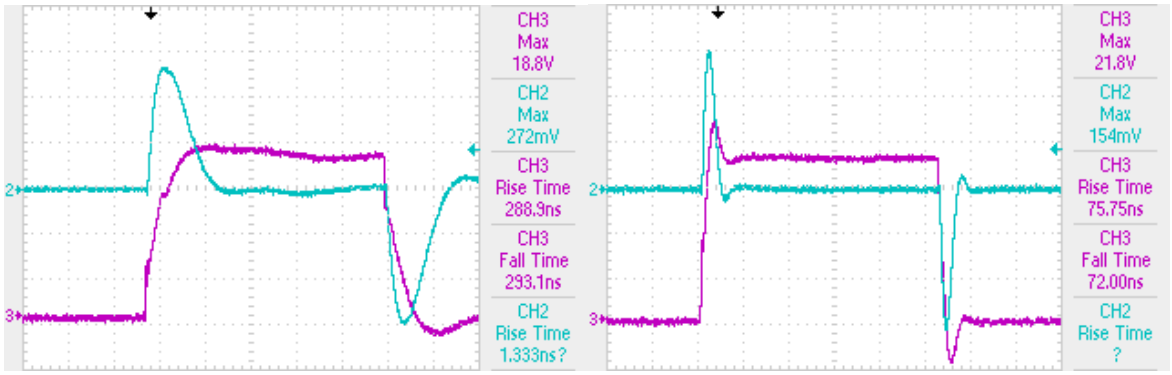

Figure 3.11. Gate voltage and current of the IXBX55N300 (left) and the CM600HA24A (right) driven by the MC4451 (12 A) chip; Voltage: CH3, 5 V/div; Current: CH2, 50 mv/A;Time 500 ns/div.

The results show that increasing the current capability from 9 A to 12 A has no significant effect and fails to improve the rise or fall time because the switches have drawn even less current than 9 A. As can be seen in Fig. 3.11, the IXBX55N300 has drawn a maximum of 3 A while the CM600HA24A drew about 5.4 A.

The main idea for increasing the rise time was to push more current to the gate to reduce the transient time assuming a constant gate charge. To achieve this goal, one of the tests included the addition of more chips in parallel in order to drive a single IGBT, which resulted in no significant effect on the rise time. Adding a second driver chip increased the current by only 10 %. The MIC4451 chip was implemented in order to drive the IGBT at 1 kV and 120 A as a means of confirming this finding. Table 3.4 shows the results of the test when several chips were used to drive a single IGBT compared with using only one chip.

Table 3.4. Effect of the number of driver chips in parallel on the rise and fall times for the CM600HA-24A.

Number of Chips Connected in Parallel	IGBT Gate Peak Current	Rise Time	Fall time
1	4A	250-290 ns	270-290 ns
2	5 A	280-290 ns	270-290 ns
3	5.5 A	280-290 ns	280-290 ns

Reference [71] developed an enhanced driver circuit while this circuit was not used as a basis for the current research; it is included as an illustration of one method of enhancing rise and fall times. They increased the rise time speed by increasing the gate voltage. The gate voltage has been stepped up to 20V for short time. Hence, IGBT draws more current and, in consequence, according to Eq. (3.3.1), the rise time becomes faster. Fig. 3.12 shows the driver circuit.

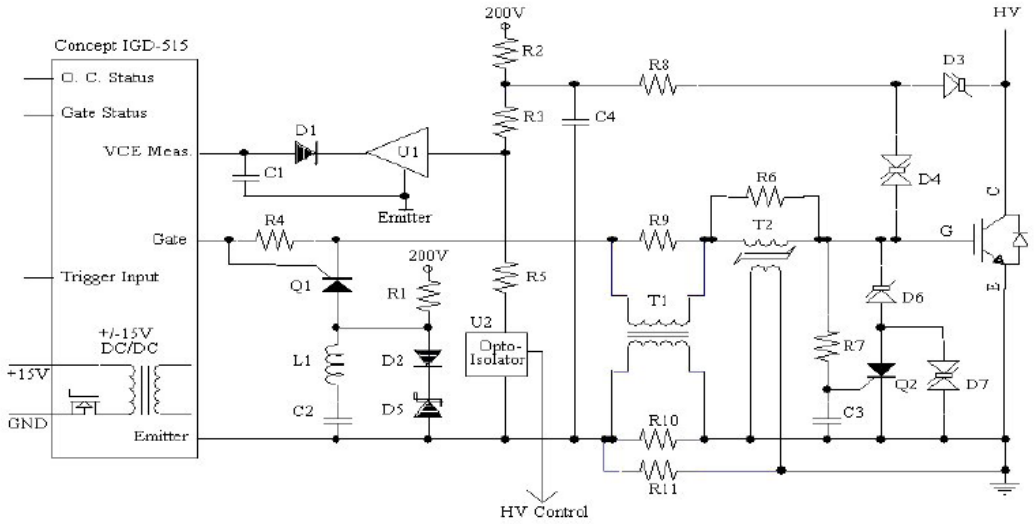

Figure 3.12. Schematic of enhanced IGBT driver circuit [71].

In this circuit as soon as the gate voltage becomes high, the current in R_4 increases and the voltage drop on R_4 turns thyristor Q_1 on and pushes the current of the pre-charged capacitor C_2 into the gate of the IGBT. This technique can boost the current of the gate up to 22 A. After turning the switch on at the boosted voltage the remaining time gate voltage is clamped to a lower voltage for short circuit

protection. This procedure was implemented using transzorbs D_6 and D_7 with control of thyristor Q_2. An additional consideration is di/dt short circuit protection. The rate of change of the emitter current is captured using R_{11} and the gate voltage drops using transformer T2 in case of a short circuit occurs. Transformer T_1 damps the oscillations. Last but not least, desaturation is detected using feedback from the collector voltage to sense the voltage rise when the IGBT is on in order to protect the circuit from short circuiting. Due to the short duration of the output waveform, the detection level was increased to 150 V rather than the typical 15 V. These considerations should be applied to the existing setup in order to enhance the rise and fall times. However, it is not possible to exceed a specific point for each switch. To achieve a faster rating, one solution was to use smaller, high voltage IGBTs. Powerex Company manufactures such an IGBT (QIS4506001) with small a die and high voltage for pulsed applications.

3.4 Driver Circuit Power Supply

Although each driver circuit needs a power supply, because the ground of stage N in the generator is the high voltage output of stage N-1, the power supplies cannot be grounded and fed to the circuit. An isolation transformer is therefore needed between each stage. The next stages must also to be isolated from the two previous stages, so transformers must be cascaded up to the last stage. The transformers have no gain and only provide isolation between the ground point of each stage. Fig. 3.13 shows how the transformers are connected. The insulation level of each transformer is 3 kV. This part of the design was implemented by Yatong Yu in a previous research project [66]. The system was designed and implemented to test motor insulation coils which required a high voltage and a low peak current in order of 70 A while, in this thesis, a high voltage and a high peak current about 1.6 kA are required for the PEF application.

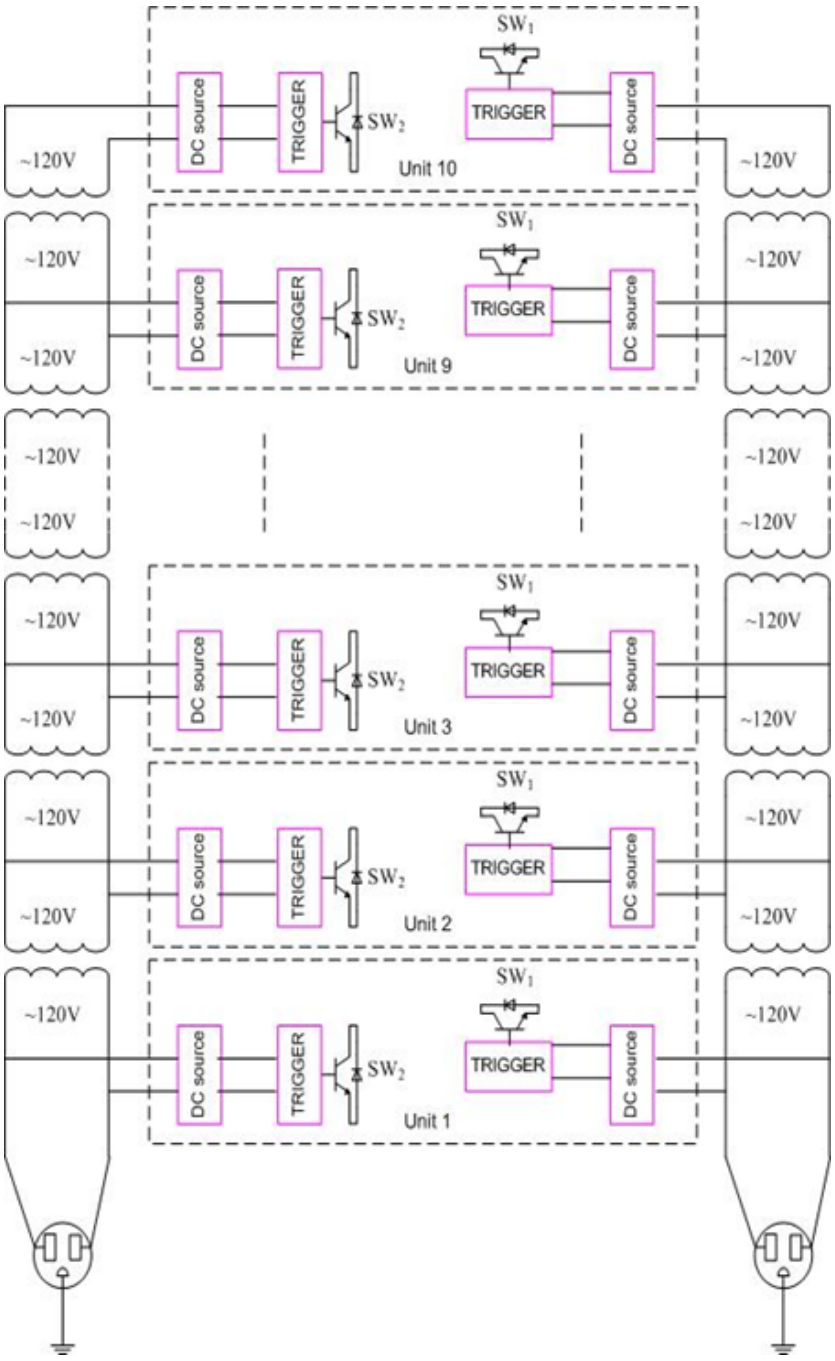

Figure 3.13. Schematic of the driver circuit power supply used by Yu[66].

Chapter 4
Controller Unit

This chapter presents the controller unit design, which is comprised of a microcontroller, a display, a keypad, a protection circuit, and optical isolators.

The gate signals for the switches, protection, frequency of the pulses, pulse width, and test duration are controlled by this unit. The design is based on a PIC microcontroller (PIC16F877A). The interface includes a 2×16 LCD display and a 4×4 keyboard. Fig. 4.1 shows a block diagram of the controller unit, which was implemented by Yatong Yu at the University of Waterloo for low current HV power modulator and has been modified and reconfigured for this project [66].

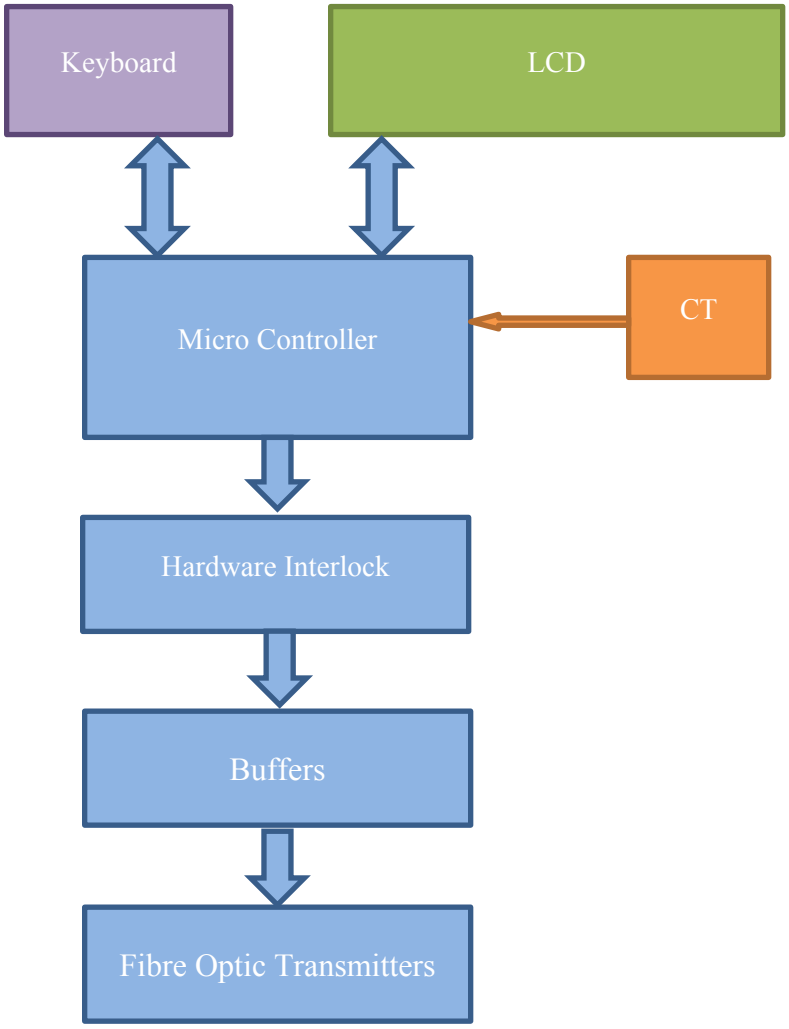

Figure 4.1. Block diagram of the controller unit.

4.1 Microcontroller

The PIC16F877A is an 8-bit PIC microcontroller chip selected as the core control element in the generator. The main specifications of the chip are as shown in Table 4.1. Table 4.2 shows the location and arrangement of the connections from the microcontroller's pin to the circuit components. Fig. 4.2 shows the architecture and capabilities of the chip.

Table 4.1. PIC16F877A specifications.

Parameter	Value
Operating frequency	DC – 20MHz
Flash program memory (14 bit words)	8K
Data memory (bytes)	368
Interrupts	15
Timers	3
I/O ports	5
Capture/ Compare/ PWM modules	2
10-bit A/D modules	8 input channels
Analog comparators	2
Instruction sets	35 instructions
Packages	40 pin

Table 4.2. PIC microcontroller chip pin connections.

Name	Port	Pin #	Description
LCD_DATA	Port B.0 ~ B.7	33 ~ 40	**Set of pins to transfer data between MCU and LCD**
EN	Port C.7	26	**LCD Enable control line**
RW	Port C.6	25	**LCD Read/Write control line**
RS	Port C.5	24	**LCD Register Select control line**
LED1	Port C.4	23	**LED output, which is on while the output waveform is generating**
KEYS	Port D.0 ~ D.3	19 ~ 22	**Set of pins to read user input from the keypad**
	Port D.4 ~ D.7	27 ~ 30	**Set of keypad scanning output**
POUT1	Port C.1	17	**Charging signal output**
POUT2	Port C.2	16	**Discharging signal output**
MANUAL	Port C.3	18	**Manual Switch, which turns the output waveform on while the button is pressed in manual mode.**
STOP	Port C.0	15	**Stop Switch, which halts the test when the button is pressed**
CURRENT	**Port A.2**	**4**	**Analog Current monitor using CT**

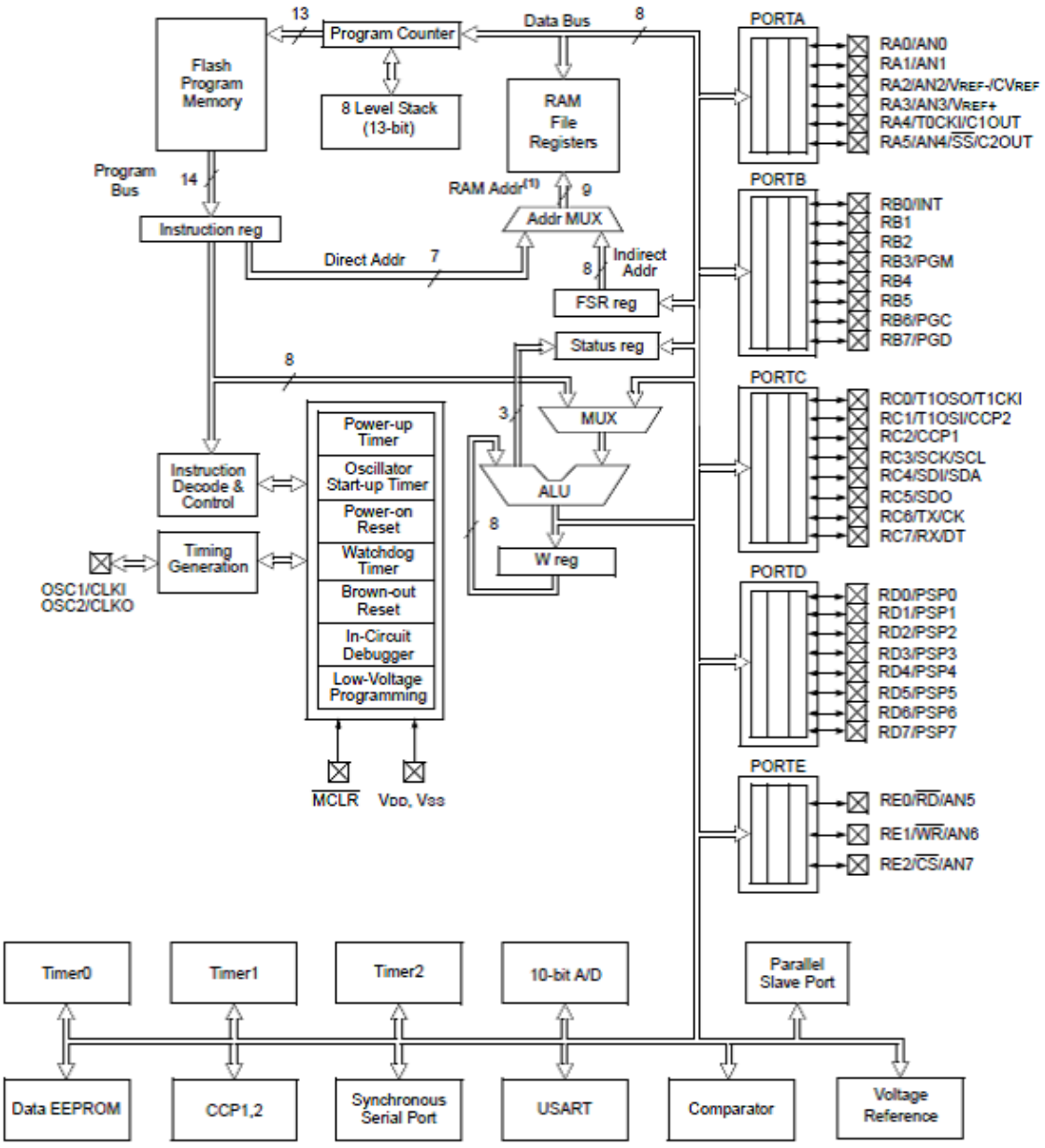

Figure 4.2. PIC16F877 microcontroller block diagram [72].

Although Ports C.1 and C.2 have multiple functions, and they can be programmed for functionalities such as capture module input, compare module output, or PWM module output, they are programmed as simple output in order to generate pulsed waveforms: C.1 generates the charging signal while C.2 generates the discharging signal. Because two signals might be turned on at the time during the reset process or in the case of a fault, an external hardware interlock has been implemented in order to prevent the switches from being turned on at the same time.

Port A.2 has been configured as an analog to digital converter in order to capture the output current. If a fault occurs, the converted digital value exceeds a preset value, indicating that a fault has happened. The program then shuts the generator off.

Ports C.0 and C.3 are programmed as a manual stop and start, respectively. Pushing the button produces a digital '1' at the input of the pin and causes the program to stop the generator.

4.2 LCD

A 2×16 liquid crystal display (LCD) is used as a monitoring device for displaying the settings and status of the system. The module accepts some standard data characters, which can be displaying on the screen, and some commands, such as turn on and off the cursor, clear the screen, select an active line, and select the position of the characters. A special command permits the status of the module to be read. The module uses an 8-line data bus (DB0-DB7) and 3 control lines (RS, R/W, E) to communicate with the other devices. A register select (RS) pin determines whether the content of the data bus is a data type or a command type. The read/write (R/W) pin should be "1" in the read state and "0" for the write state. As can be seen in Fig. 4.3, after the distention register is selected by the RS pin and read or write is selected by the W/R pin, the enable (E) pin should be turned on for a specific time and data should be loaded onto the data bus at this point. When the enable pin goes off, the data latches to the LCD for the write process and is ready in case the read process is required.

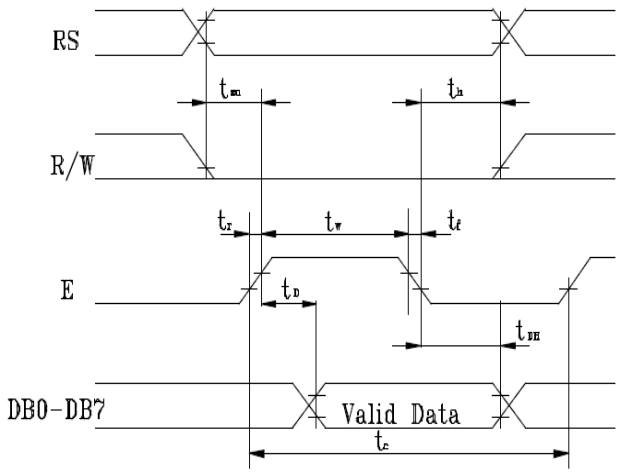

Figure 4.3. LCD read and write timing.

The remaining pins are dedicated to power, the LCD back light, and screen contrast. The internal block diagram of the LCD is shown in Fig. 4.4.

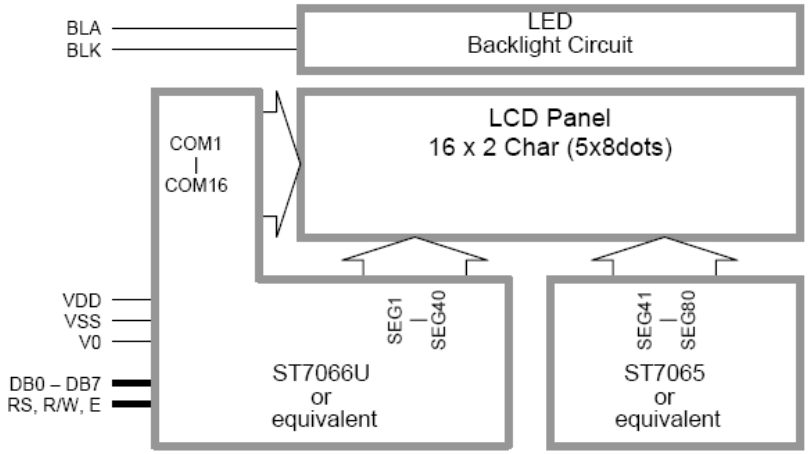

Figure 4.4. Block diagram of the LCD.

4.3 Keypad

The user can set the initial settings using a 4×4 matrix-type keypad. Fig 4.5 shows the keypad map. One of the columns is set at the same time that are connected to the D.4~D.7, and rows that are connected to D.0~D.3 are read as input. This polling is continued by changing the column that was set at the previous stage. As soon as a user presses a button, the corresponding row and column are connected and can be read at the input row. Each row has a pull-up resistor of 10 kΩ.

Row 4	1	2	3	A
Row 3	4	5	6	B
Row 2	7	8	9	C
Row 1	*	0	#	D
	Col 1	Col 2	Col 3	Col 4

Figure 4.5. 4 by 4 keypad configuration.

4.4 Protection Circuit

This section uses a current transformer (CT) with ratio of 0.01 V/A in order to record the current at the output. The analog signal is fed into an analog to digital converter (A/D) of the microcontroller using matching components. A threshold is preselected as the fault level. As soon as the signal passes the fault level, the microcontroller shuts off the IGBT gate signals to prevent further damage.

4.5 Firmware

The firmware of the pulse generator is written in the assembly language of the PIC microcontroller in the MPLAB environment. Fig 4.6 shows the flow chart of the program. After the program is started, it shows an initial greeting and then proceeds to the parameter import unit. Using the keyboard, the user enters the pulse width, frequency, mode of operation, and duration of the test. The program then starts the waveform generation loop for the specified time. In the case of a fault, it shuts the signal off and waits for the user to restart the program.

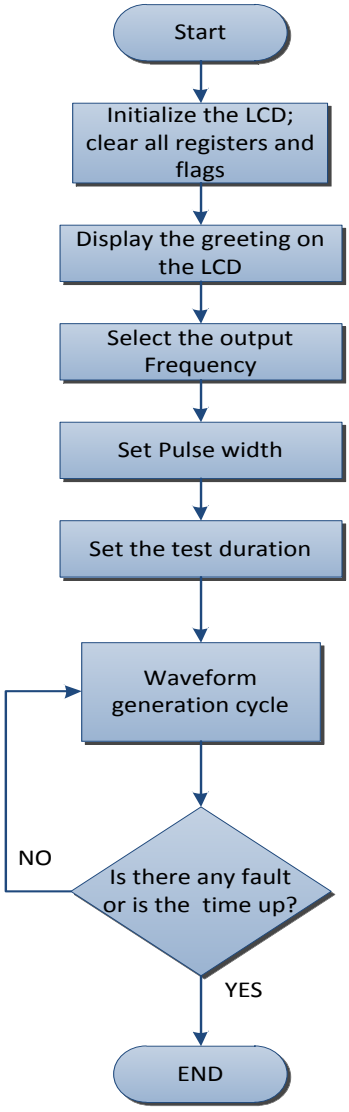

Figure 4.6. Flow chart of the firmware program.

4.5.1 Pulsed Waveform Generation

One of the timers in the microcontroller was used to generate the charging and discharging signals. Timer0 is an 8-bit timer-counter module that can be used in different modes. A block diagram of the timer is shown in Fig. 4.7. In the timer mode, it uses the system clock multiplied by a pre-scalar register as the input clock for incrementing the timer data register (TMR0) in each clock. Once the TMR0 value reaches a specific value or reaches the top value, an interrupt signal is generated. The frequency of this interrupt is input by the user at the beginning of the program.

In the timer interrupt service routine, both the charging and discharging signals are generated. At the beginning of the interrupt routine, the charging signal is ON and the discharging signal is OFF. At this point, the charging signal is set to OFF to end the charging process. A delay has been implemented in order to produce a gap between the charging state and the discharging state. The discharging signal is then turned ON for a specific duration that has been previously set by the user as the pulse width, and it is turned OFF after that period. The discharging signal is followed by another delay gap, at the end of which the charging signal is set to ON again, and the interrupt is terminated until the next.

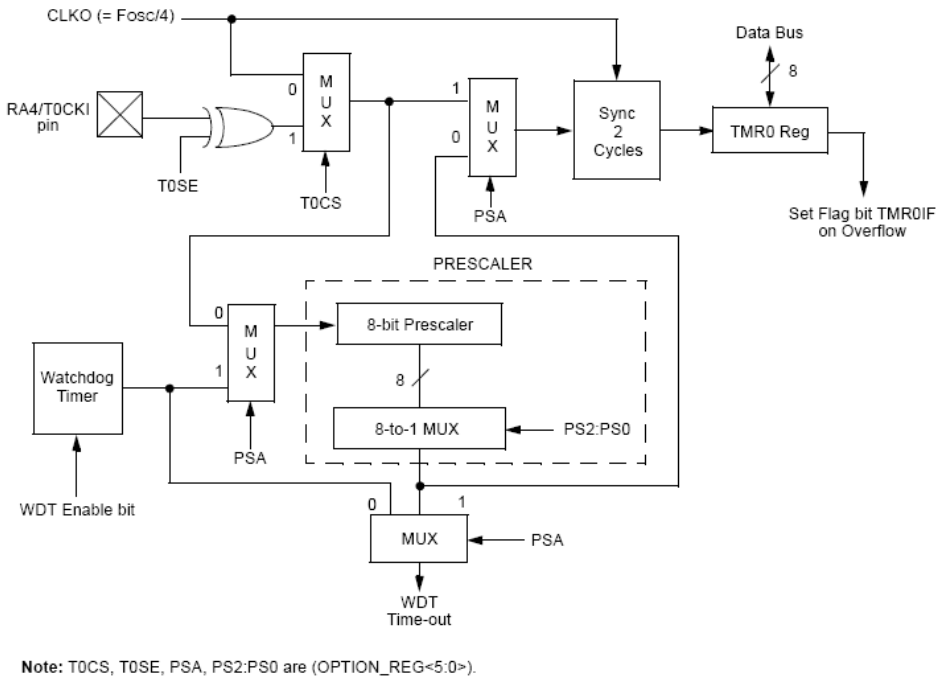

Note: T0CS, T0SE, PSA, PS2:PS0 are (OPTION_REG<5:0>).

Figure 4.7. Block diagram of timer 0

Chapter 5
Results and Discussion

The high voltage pulse generator for food treatment was implemented for two stages and tested for different configurations and situations. The design of the generator was explained in the previous chapter. This chapter presents the results of the testing, a discussion on the performance of the generator, and a comparison of the results with those obtained in other research.

5.1 Trigger Signal

The controller unit generates trigger signals according to the settings input by the user. The signals are fed to the IGBTs through a fibre optic isolator and IGBT driver circuit in order to provide a suitable current and voltage for the IGBTs. Fig. 5.1 shows the charging and discharging signals applied to the IGBTs for one stage.

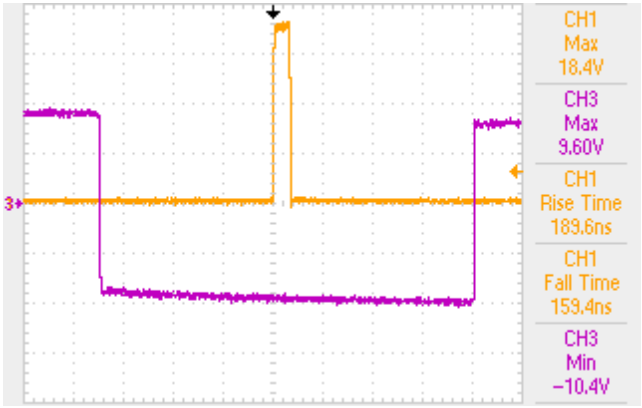

Figure 5.1. IGBT gate voltages for charging (CH1, Orange) and discharging (CH3, Purple); voltage: CH1 5 V/div; current: CH3 5 A/div; time: 10 µs/div.

The discharging signal has a high amplitude of around 18 V and a low amplitude of zero. The signal was generated using either a TC4421 or MIC4451 chip. The pulse width is adjustable by the user; in this case, it was set at 5 µs. As can be seen, the charging signal is covered by a dead time in the discharging signal, which is at about 30 µs on each side in order to prevent complementary switches from turning on at the same time. The level of the charging signal is -10 V in the OFF state and 10 V in the ON state. The signal was generated using a TD351 driver chip, which was used only for the charging switches due to its lower current ratings.

5.2 Output Waveform

When the IGBT gate signals are ready, it is possible to raise the DC link voltage to charge up the capacitors and then discharge them on the load in series at the output of the generator. Fig. 5.2 shows the typical waveform of the generator for pulse widths of 3.5 µs and 5.8 µs when apple cider is used as the liquid to be treated. The peak voltage is 5.2 kV, and the peak current is 1.18 kA; the configuration is two stages with two switches in parallel in each stage. The flat top is decaying due to the load resistance and generator capacitance. With larger pulse widths, the decaying flat top is more noticeable. If the load is assumed to be a purely resistive load, the equivalent resistance in the chamber is 4.4 Ω. Considering that the total capacitance of the generator is 3 µF, the RC time constant would then be 13.2 µs, calculated as follows:

$$\tau = RC = 4.4 \times 3\mu F = 13.2\mu s \qquad (5.2.1)$$

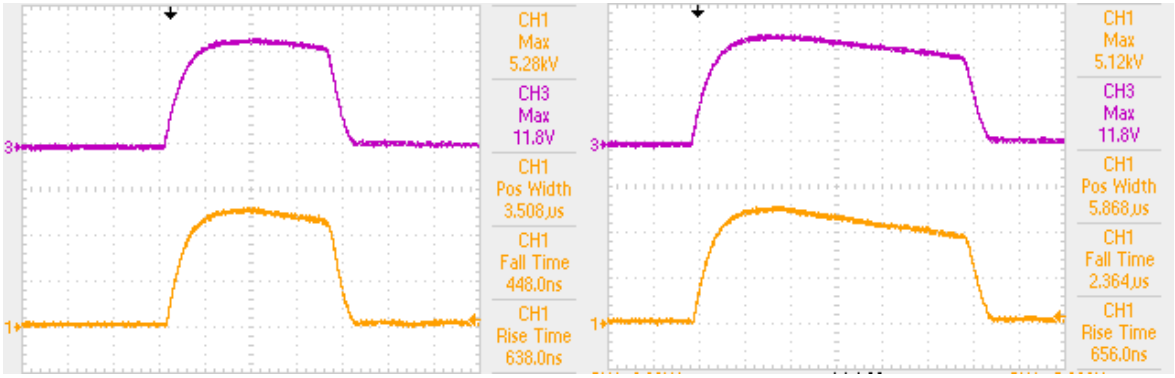

Figure 5.2. Waveform with output voltage (CH1: 2 kV/div) and current (CH3: 500 A/div) for 2 switches in parallel and a 2-stage configuration for different pulse widths: 3.5 µs (left); 5.8 µs (right); time 1µs/div.

These results can be compared with output waveforms produced by generators presented in the literature. Fig. 5.3 shows the output voltage and current waveform of the generator developed at Ohio State University [48]. Although the amplitude of the voltage is about 7 kV, the current capability is as low as 50 A, which is very low compared with the results obtained with the new generator presented in this research: up to 1.6 kA. The rise and fall times seem to be similar. In addition, the scalability of the Ohio State design is limited due to their use of a pulse transformer.

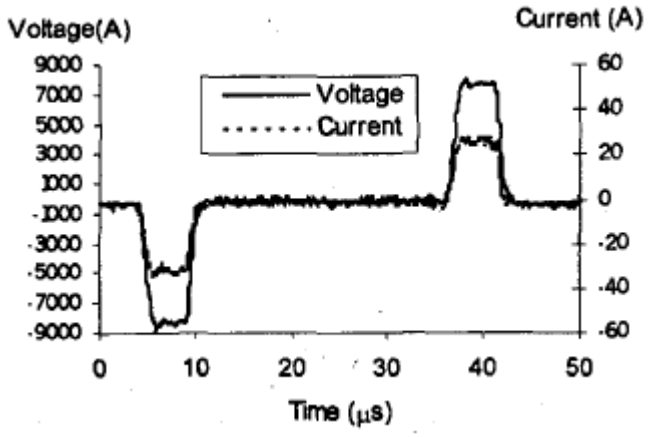

Figure 5.3. Voltage and current waveform of the Ohio State University pulse generator [48].

Cheng et al. [45] also reported similar results using a pulse generator based on hybrid flyback converters. They reported voltages as high as 26 kV with an output current of around 50 A, as shown in Fig. 5.4. However, the pulse width is very short, about 200 ns, and the rise time is about 100ns, which is very good. The constraints of this design are the complexity of the generator design and the low current capability.

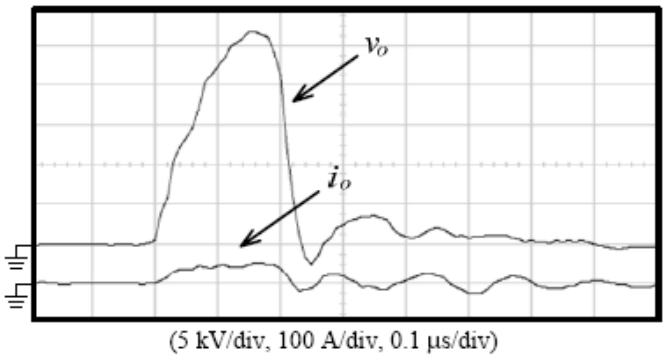

Figure 5.4. Voltage and current waveform of the pulse generator developed by Cheng et al. based on a flyback converter [45].

Beak et al. [49] used a concept similar to the one in this research. They employed IGBT switches in a Marx generator configuration to produce 20 kV and 300 A at the output, as shown in Fig. 5.5. The output is square and the rise and fall times are around 1 μs, which are slower than the results obtained for this thesis. The main drawback of their design is the lack of control of the charging process, which causes a limited output current or a maximum frequency, as shown in Fig. 1.5.

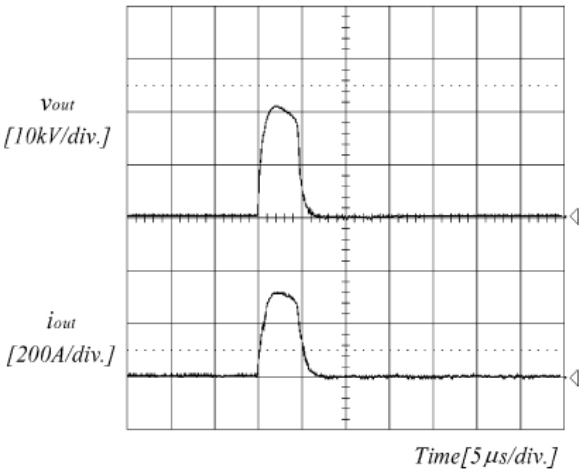

Figure 5.5. Voltage and current waveform of the pulse generator developed by Beak et al. based on a solid state Marx generator [49].

Fig. 5.6 shows the output voltage waveform of a pulse generator using two stages of MOSFETs in series [46]. The output square waveform and the rise and fall times are all appropriate, but the current rating is very low, and the generator can be used to treat only a small amount of liquid, in the order of several mL. Larger switches should be used to handle a higher voltage and current.

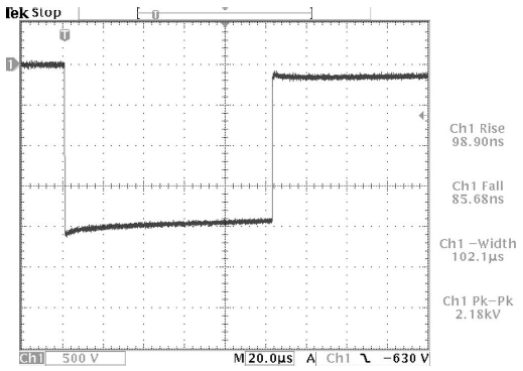

Figure 5.6. Output voltage waveform of the pulse generator developed by Grenier et al. based on MOSFETs in series [46].

The output waveform of the pulse generator produced by Diversified Technology [52] is shown in Fig 5.7. As mentioned, they used a chain of IGBTs in series and reported very good results: they generated a 20 kV, 35 A square waveform with a rise time of ~200 ns. The current is still low, and they could have used IGBTs in parallel to enhance the current capability. They employed newly developed IGBT switches manufactured by POWEREX, which were developed specifically for pulsed power applications. Using these switches can help to achieve smaller rise and fall times. Prins et al. [57] also reported similar results.

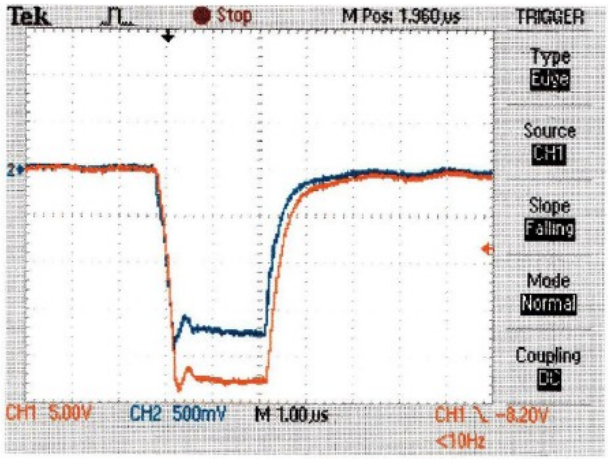

Figure 5.7. Output voltage waveform of Diversified Technologies's pulse generator based on IGBTs in series [52].

Nguyen et al. [71] developed an enhanced drive circuit, as described in Chapter 1. They reported an output square waveform of 2.2 kV and 3 kA, as shown in Fig. 5.8. The voltage rise and fall times are around 400 ns, which, relative to the peak voltage and current, can be considered very fast. The pulse width is about 3 µs. Their results confirm that enhancing the drive circuit, as shown in Fig.3.12, by pushing more current to the gate and raising the gate voltage even higher than the switch ratings, can improve switching performance. They used their design for electron accelerator applications.

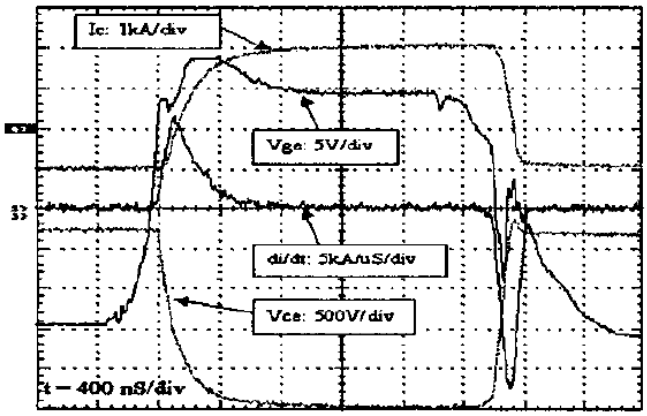

Figure 5.8. Output voltage waveform of an IGBT driven by an enhanced driver circuit, developed by Nguyen et al. [71].

At the University of Missouri, researchers used a magnetic pulse compressor [44], as discussed in Chapter 1, in order to generate a short-duration decaying impulse waveform, as shown in Fig. 5.9. The voltage amplitude was as high as 20 kV and the peak current was reported to be 860 A. However, the duration of the pulse was 1000 ns, because the decaying impulse, the useful part of the waveform

was 258.6 ns, which is a common constraint of decaying impulse waveforms. As well, changing the output pulse width is also difficult due to the design principles on which magnetic compressors are based. Other researchers have produced pulse generators with decaying impulse output waveforms that have low energy efficiency and a high temperature rise in the liquid compared with those produced by square pulses with the same energy applied [35, 36, 37].

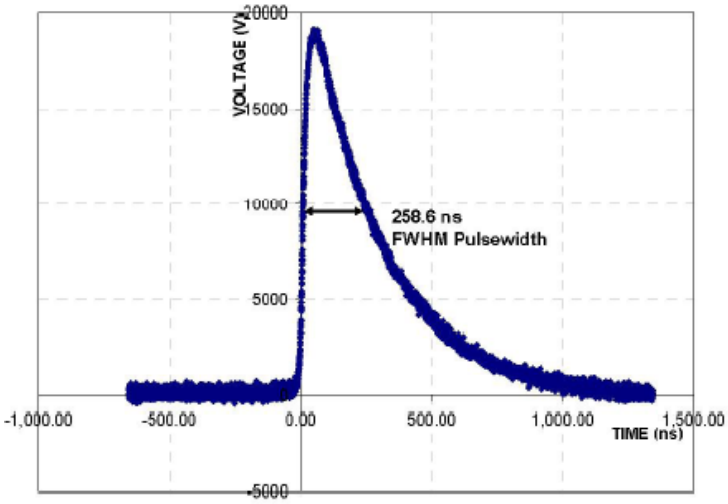

Figure 5.9. Output voltage waveform of a pulse generator based on a magnetic compressor [44].

If the pulse width applied becomes more than the RC constant associated with the equivalent resistance of the liquid in the chamber and the generator capacitance, the output waveform is more like a decaying impulse than a square pulse, as shown in Fig. 5.10. In these tests, the peak voltage is 5.8 kV and the peak currents are 1.14 kA and 1.7 kA. Although the generator pulse width is 10 µs, the output voltage reaches 50 % only at 5 µs, as in Fig. 5.10a. Hence, to achieve a more efficient treatment for a liquid with this conductivity, the pulse width should be less than 5 µs, and the applied energy can kept constant by increasing the frequency or treatment time. Fig. 5.10b shows the output waveform for 5 µs. These results are more efficient than those with a decaying impulse waveform similar to the one in Fig. 5.9. Based on the 13.2 µs RC time constant from Eq. 5.2.1, the efficiency of the generator is much higher than that of a decaying impulse generator, given the same conditions.

Another important observation is related to the switch current. In Fig. 5.10, CH3 and CH4 measure the switch current while CH3 measures the total output current of the generator (the current passing through both switches), and CH4 measures the current of one switch at the top stage. Considering the current transformer ratios and the oscilloscope division setting, CH4 shows the amount of the current to be twice that of CH3. Therefore, when CH3 and CH4 have the same amplitude as that shown in

Fig. 5.10 (a) and (b), then the total current measured is twice the current of one switch. This test shows that two switches have equal current distribution, that the positive temperature coefficient is enough to balance the current, and that no additional circuits are needed.

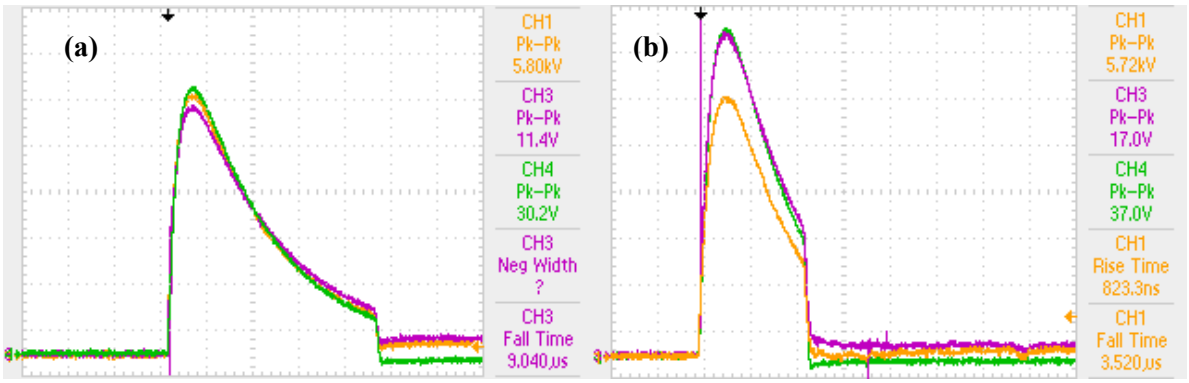

Figure 5.10. Output waveform of the generator with a 4.4 Ω load in 5.8 kV with large pulse widths (a) 10 µs (b) 5 µs; voltage: CH1 1 kV/div; current: CH3 200 A/div, CH4 100 A/div; time: 2.5 µs/div.

5.3 Rise and Fall Times

Different configurations result in different capabilities. A higher number of stages increases the maximum output voltage while adding parallel switches increases the maximum output current. Fig. 5.11 shows the output waveform for a two-stage configuration with two switches in parallel in each stage for liquids with different conductivities. The figure shows that the rise time is slow for highly conductive liquids, such as tomato juice, while it is at a reasonable level for other liquids. The voltage and current levels were kept below the rating of one switch in order to enable a comparison of all the possibilities. This test was repeated for the following configurations: one stage with one switch, one stage with two switches in parallel, one stage with three switches in parallel, two stages with one switch, and two stages with two switches in parallel.

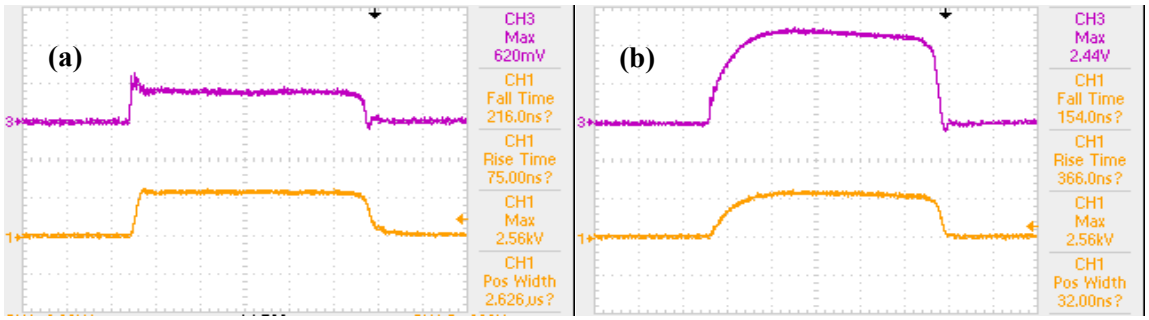

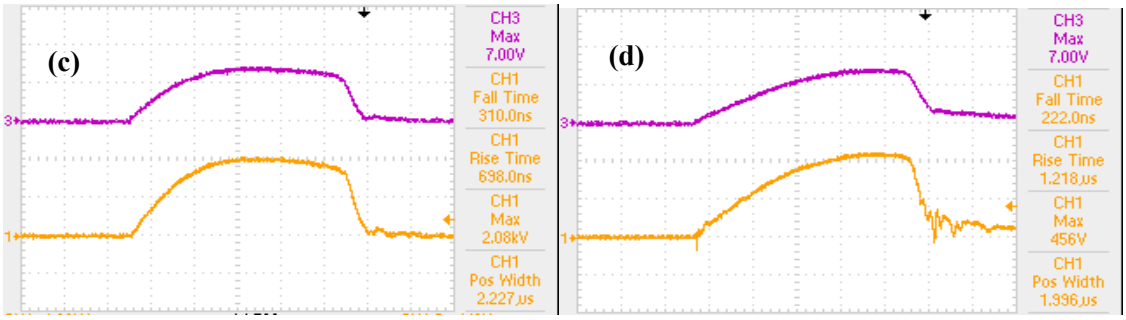

Figure 5.11. Output voltage (CH1) and current (CH3) waveform for 2 switches in parallel and a 2-stage configuration for different load conductivities: (a) 200 µS/cm voltage: CH1 2 kV/div, current: CH3 50 A/div(b) 1000 µS/cm voltage: CH1 2 kV/div, current: CH3 100 A/div (c) 3300 µS/cm voltage: CH1 1 kV/div, current: CH3 500 A/div (d) 15 000 µS/cm voltage: CH1 200 V/div, current: CH3 500 A/div; time: 500ns/div.

All of these configurations were tested with different conductivities in order to study the effect of the configuration and the conductivity of the liquid on the rise and fall times. The results are shown in Fig. 5.12. As can be seen, adding more stages increases the rise time while adding more parallel switches decreases the rise time. The difference is greater in higher-load currents. While the differences in rise times are not very large, the best time can be seen with the configuration that includes one stage and three switches in parallel, while two stages and one switch produced relatively slower transient which can be improved by minimizing series inductance in the circuit. Table 5.1 shows all the values recorded.

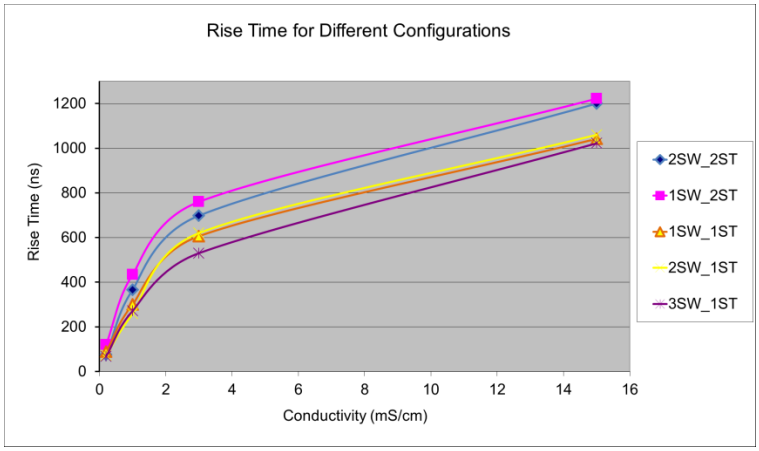

Figure 5.12. Rise times under different conductivities and configurations (SW = number of switches in parallel; ST = number of stages).

Unlike the rise time, which changes with the conductivity of the load, the fall time exhibits small changes if the fall times for low-conductivity loads are excluded. Such an exclusion is reasonable because the small capacitance of the chamber can affect fall time readings for very low

conductivities. The long fall times for liquids with low conductivities shown in Fig. 5.13 could therefore be a result of chamber capacitance rather than the process of turning the switch off. The remainder of the fall times were between 100 ns and 400 ns.

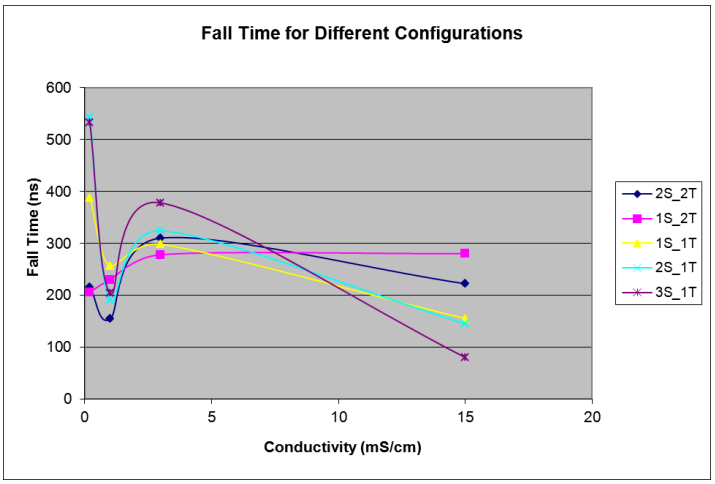

Figure 5.13. Fall times under different conductivities and configurations (SW = number of switches in parallel; ST = number of stages).

Table 5.1. Rise and fall times under different conductivities and configurations.

	2 switch 2 stages		**1 switch 2 stages**		**1 switch 1 stages**		**2 switch 1 stages**		**3 switch 1 stages**	
	Rise	Fall	Rise	Fall	Rise	Fall	Rise	Fall	Rise	Fall
200	75	216	120	206	88	388	72	542	68	532
1000	366	154	434	230	300	256	258	190	271	204
3300	698	310	760	278	606	298	620	324	530	378
1500	1200	222	1222	280	1042	155	1060	145	1022	80

These results can also be viewed from another perspective. Fig. 5.14 shows the rise time levels for two extreme conductivities of 200 µS/cm and 15 000 µS/cm, for a number of circuit configurations. It also shows, however, some small differences in rise times with changes in the conductivity; the results are consistent with regard to the configurations. It can be concluded that changing the number of switches has no significant effect on the rise time, but adding a stage can increase it. Therefore, consideration must be given to minimizing the path resistance and inductance during the implementation of the next stages.

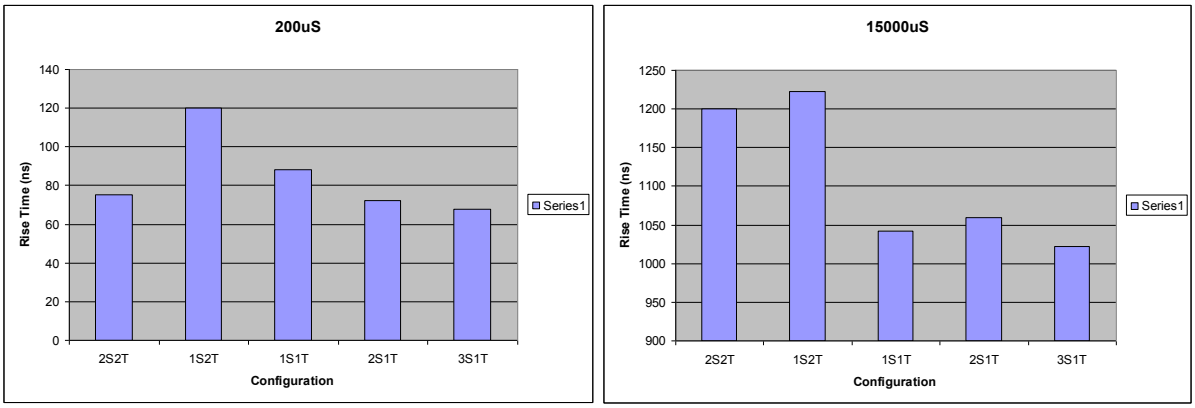

Figure 5.14. Rise times with different configurations under load conductivity (a) 200 µS/cm and (b) 15 000µS/cm.

Fig. 5.15 shows how the rise/fall times change with the conductivity of the liquid for a configuration with one stage and three switches in parallel under 2 kV pulses. The best performance of the system is with a liquid conductivity of 200 µS/cm to 500 µS/cm because the summation of the fall and rise time values is minimal in this range. The rise time increases when the conductivity is higher because the current density is higher, and in consequence, more time is required for the carriers in the switch to conduct the total amount of the current. On the other hand, the fall time decreases with increases in the conductivity due to the characteristics of the switch and also to the smaller resistance and the resulting smaller RC constant during the turning off condition, as previously mentioned.

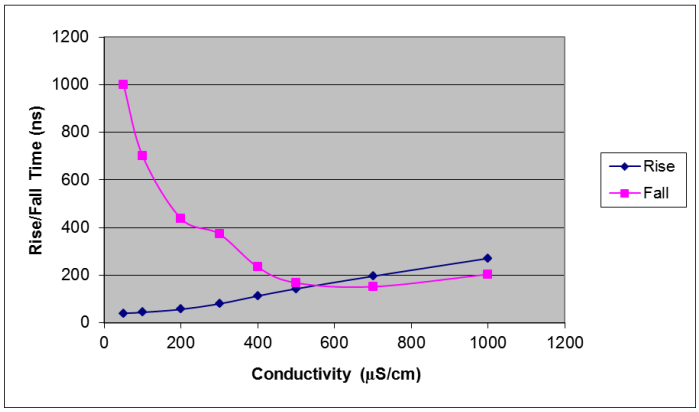

Figure 5.15. Changing rise and fall times with different load conductivities for 2 kV on a configuration with 3 switches and 1 stage.

Several types of switches were compared. The Powerex IGBT (CM600HA-24A) rated for 1.2 kV and 600 A was replaced with an IXBX55N300. Both switches were energized under 1 kV pulses with different conductivities, ranging from 50 µS/cm to 15 000 µS/cm. The rise and fall times were

recorded for each case, as shown in Fig.5.16. Both switches were driven by an MIC4451 (12 A) chip. The results show that the rise time with the CM600 is faster than with the IXBX55N300, while the fall time with the IXBX55N300 is faster than with the CM600. It should be noted that the summation of the rise and fall times is approximately constant in both cases. Moreover, neither result is very satisfactory, with values ranging from 200 ns to1000 ns. It seems that implementing a more sophisticated driver circuit is necessary in order to achieve a faster transient, as shown in [71], or that switches must be replaced with smaller switches capable of handling the pulse conditions as implemented by Diversified Technologies [52], who used newly developed IGBTs for applying pulsed power and reported rise times as low as 200 ns. However, they reported this rating with a low current of about 35 A, which is similar to the results obtained for this thesis research with conductivities below 500 µS/cm. With respect to the current level implemented in [71], a faster rise time of about 400 ns was reported for a 3 kA current, compared with the current thesis results of 1000 ns for a 1 kA current.

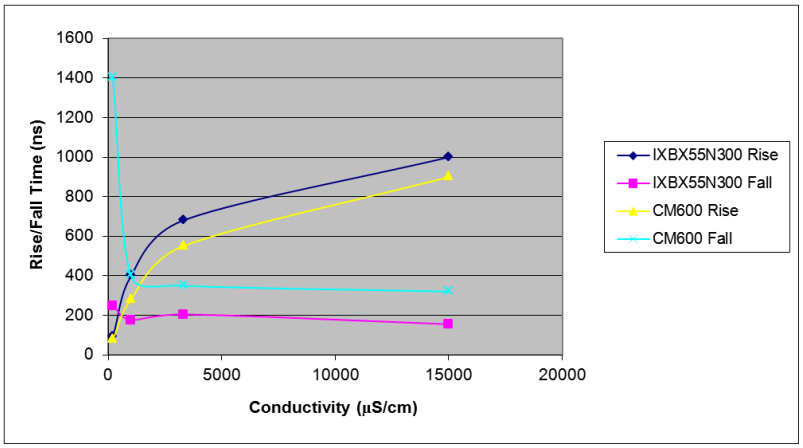

Figure 5.16. Comparison of the IXBX55N300 (3 kV, 55 A IGBT) and the CM600HA-24A (1.2 kV, 600 A IGBT) with respect to rise/fall times with different load conductivities.

5.4 Effect of Pulse Width on Temperature Rise

A square pulse voltage of 5.1 kV and 3 Hz was applied to the 1.27 mm gap in the treatment chamber, which resulted in a 40 kV/cm electric field across the liquid. With apple cider as the treatment liquid, the peak current recorded was 1 kA through the liquid. The pulse width was changed from 1 µs to 7 µs in 10 steps.

With respect to the fact that greater energy per pulse is needed for larger pulses, larger capacitors are used. The following equation shows that the capacitor should be increased to 6 µF in order to

obtain a pulse width of 7.6 µs. The two capacitors, C1 and C2, connected in series in the discharging configuration, form a total capacitance of 3µF. The maximum output energy per pulse was thus 39 J/pulse, calculated as follows:

$$E_{max} = \frac{1}{2} C_{total} V^2 = \frac{1}{2} \times 3 \times 10^{-6} \times (5.1 \times 10^3)^2 \approx 39\, J \quad (5.4.1)$$

Assuming this maximum 39 J/pulse energy, 5.1 kV as the output square pulse voltage, and 1 kA as the load current, the maximum pulse width for the generated square pulse was 7.6 µs, calculated as follows:

$$T_{max} = \frac{E_{max}}{V \times I} = \frac{39}{5.1 \times 10^3 \times 1 \times 10^3} \approx 7.6\ \mu s \quad (5.4.2)$$

To compare the effect of pulse width on the rise in temperature, the energy applied was kept constant at 2700 J for all tests. This level of energy was selected based on the chamber size so that the temperature would change appropriately during the tests. The treatment time was varied to correspond to this energy. Fig. 5.17 shows the temperature profiles, with different treatment times for the liquid.

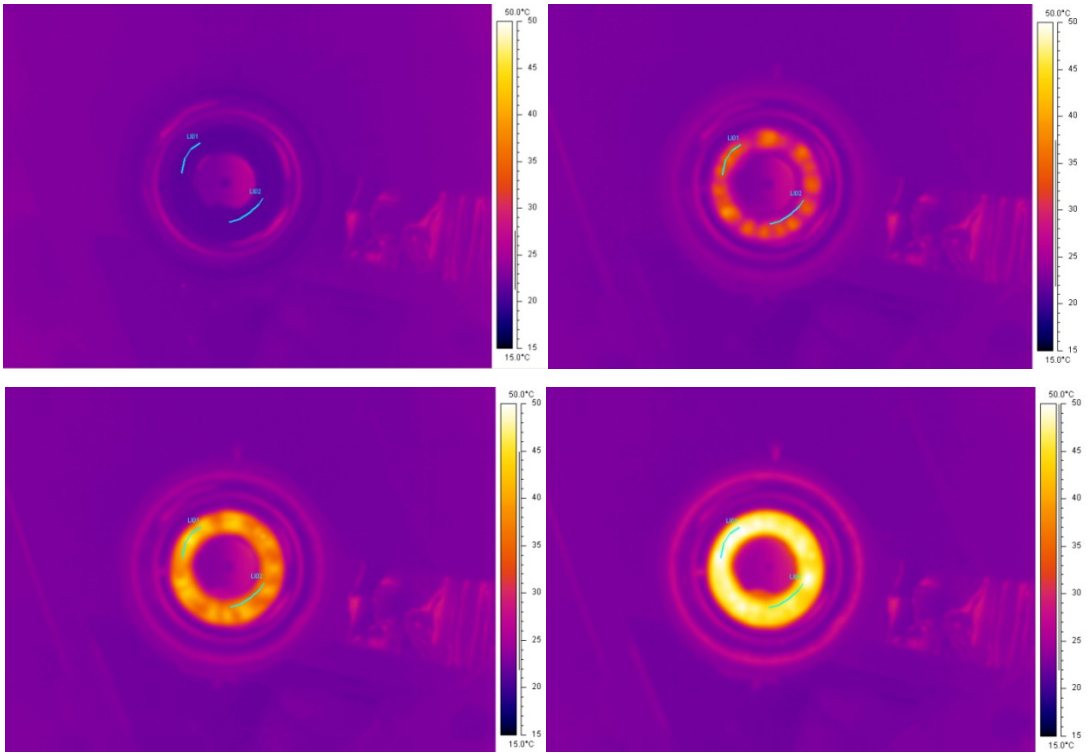

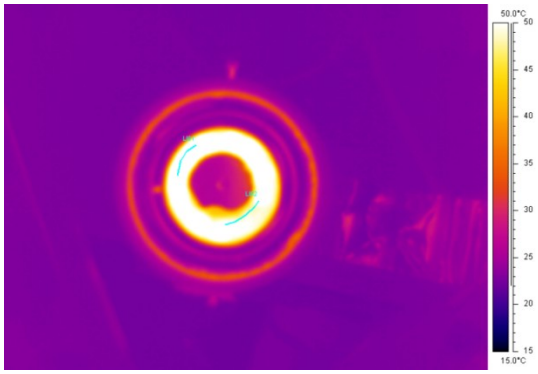

Figure 5.17. Temperature rise in alcoholic apple cider during 30 seconds with the application of 5.1 kV, 1 kA, and 3 Hz pulses with a 3.5 µs width (LI01 and LI02 represent the temperature measurement lines).

Hot spots can be seen during the rise in temperature. These hot spots may be result of roughness on the electrode surface and high field regions associated with these spots. After the passage of time, these hot spots partially disappear due to convection in the liquid. Forty-five points were placed every 8º all around the chamber in order to determine how the temperature changed in each part of the chamber. Fig. 5.18 shows the rise in temperature over time. Obviously, the temperature goes up when pulses are applied, but fluctuations in temperature rise were observed, which confirms the presence of hot spots.

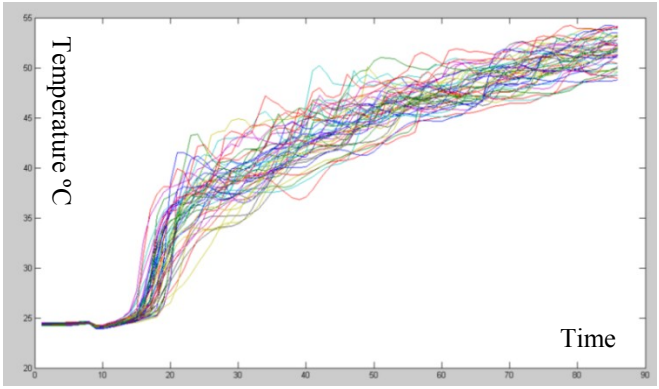

Figure 5.18. Temperature rise (ºC) in alcoholic apple cider during 30 seconds with the application of 5.1 kV, 1 kA, and 3 Hz pulses with a 3.5 µs width (each line represents one of the spots on the chamber; each horizontal point represents 0.4s).

Fig. 5.19 shows the temperature rise at each point of the chamber. Where each point represents a radial position of 360/45= 8 degrees located on the horizontal axis; the vertical axis shows the temperature (ºC); each line with a different color represents the temperature sampled at the same times.

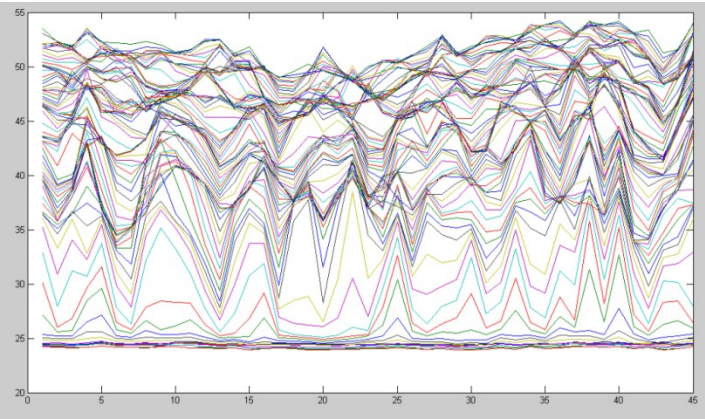

Figure 5.19. Temperature rise at each point of the chamber.

Fig. 5.19 shows the temperature rise at each point of the chamber. Where each point represents a radial position of 360/45= 8 degrees located on the horizontal axis; the vertical axis shows the temperature (ºC); each line with a different color represents the temperature sampled at the same times.

At the beginning of the test, all of the points had the same temperature and all of the lines were concentrated at 25º C. Applying the pulses caused the temperature to rise, but due to the presence of roughness, some hot spots can be clearly seen, as can the fact that measuring points 5, 10, 15, 25, etc., have significantly higher temperatures than the other points. The temperatures at these hot spots will be balanced at higher temperatures with the passage of time and because of the thermal convection in the chamber. It can be concluded that any roughness or sharp points on the chamber surface must be eliminated. Otherwise, they could affect the efficiency of the treatment or even cause a breakdown in the liquid.

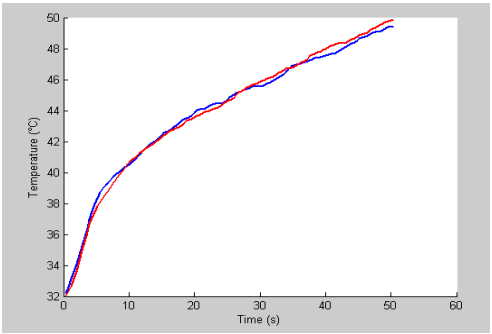

Figure 5.20. Temperature rise in apple cider with respect to time along the measurement lines (Blue = LI01; Red = LI0).

As can be seen from Fig. 5.20, the application of 2700 J over 50 seconds raises the temperature of

the liquid by 20º C above the ambient temperature. It should be noted that this amount of temperature rise is because of using the chamber without flow and the temperature can be kept low in real application. As mentioned, the tests were repeated for different pulse widths, keeping the total energy at a constant level in order to investigate the effect of pulse width on rise in temperature. The voltage was fixed at 5.1 kV with a fixed frequency of 3 Hz to fulfill the requirement for an electric field of 40 kV/cm across the liquid. The treatment time was varied to maintain a constant applied energy. Table 5.2 provides the calculated energy per pulse according to the voltage and current measurements and the total time required to reach an energy level of 2700 J for each pulse width studied. The actual temperature rise for each time was recorded in the experiments, using a pre-calibrated IR camera. The energy was calculated using recorded output voltage and current waveforms, as follows:

$$Enegy\ per\ pulse = \int V.I.dt \tag{5.4.1}$$

where V is the voltage, and I is the current waveform of the single pulse.

Table 5.2. Measured total time and energy per pulse for different pulse widths.

Pulse Width (µs)	Energy per Pulse (J)	Total Time (s)
1.1	13.59	198.74
1.5	19.52	138.30
1.9	26.18	103.14
2.7	40.77	66.22
3.5	53.69	50.29
4.3	64.16	42.08
5.1	75.99	35.53
5.9	84.15	32.08
6.7	89.78	30.08
7.1	97.27	27.76

Fig. 5.21 shows the temperature rise for different pulse widths. Despite the fact that the total energy input into the treatment liquid is maintained at a consistent level of 2700 J, it is evident that larger pulses have a greater impact on the liquid temperature rise than do shorter pulses. Furthermore, it has also been reported that pulses with a longer width can adversely affect the treated samples due to electrode reactions [18], [73]. Accordingly, it is suggested that a large number of short pulses be used rather than fewer long pulses in order to keep the temperature rise to a minimum. As the heat dissipation seems to be much better than injecting high energy using larger pulses. To optimize the

pulse width requires matching the kinetics of inactivation of the microorganisms with the temperature rise.

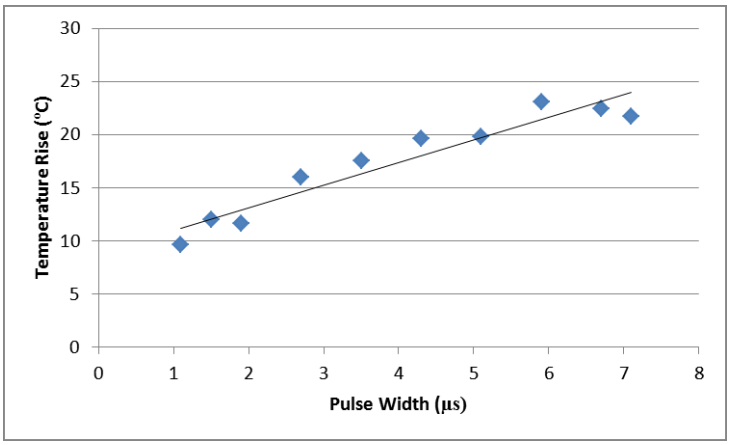

Figure 5.21. Temperature rise in the liquid with respect to pulse width.

5.5 Eliminating the Noises

Some noise was experienced during the tests. As can be seen in Fig. 5.22, oscillation occurs at the fall state, and this noise appears mostly on the current waveform. In the presence of the noise, increasing the level of the voltage above a specific value led to failure in the generator and the breaking of one of the discharging switches. A broken IGBT switch acts as a short circuit between all pins and draws a great deal of current. On the positive side, it also causes the other switches to short circuit and prevents the burning out of all the parallel switches.

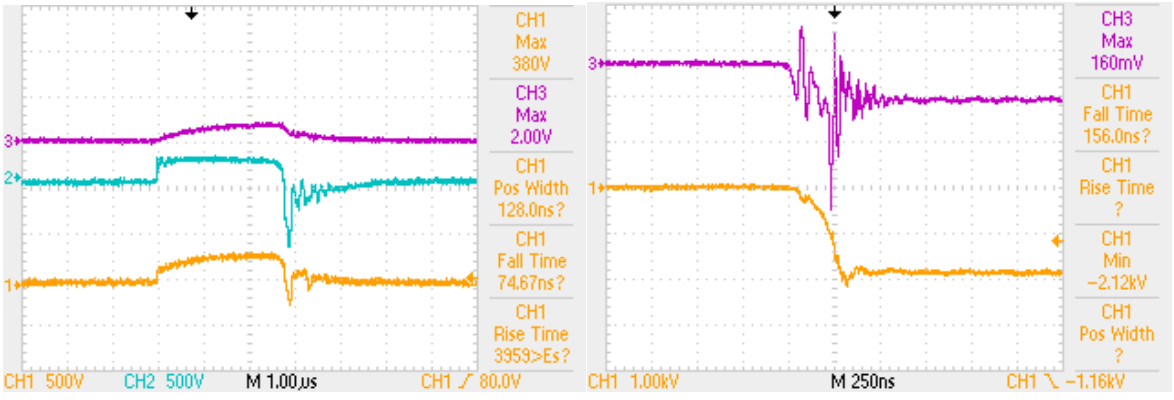

Figure 5.22. Unexpected oscillations on the waveform causing the system failure.

Several tests were conducted in order to determine the source of the noise, such as adding snubber circuits or filters. After experimentation and measurement, the reason for the problem was identified: stray inductance because of the wiring. A high voltage wire had been used to connect the parts, and

despite the ability of these wires to withstand a high voltage of about 30kV, their inductance is high. These wires were therefore replaced with copper strips, which are shown in Fig. 5.23. They have much lower inductance and can eliminate resonance in the circuit. The measured inductance of these strips is several hundred nH lower than that of the high voltage wires.

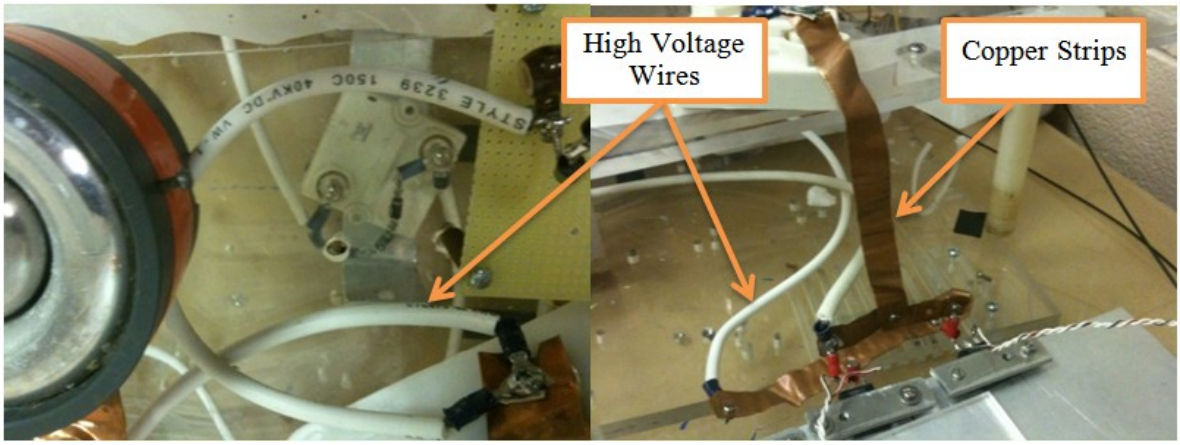

Figure 5.23. Replacing high voltage wires with copper strips to eliminate oscillations.

Another problem was noticed when the voltage was increased to more than about 3.5 kV in the configuration with two stages and two switches in parallel. An oscillating noise shown in Fig. 5.24 would appear during the rise state and cause the discharging switches to burn completely. This noise would appear at a specific voltage so that it was complicated to diagnose the problem, which also failed to appear in the simulations.

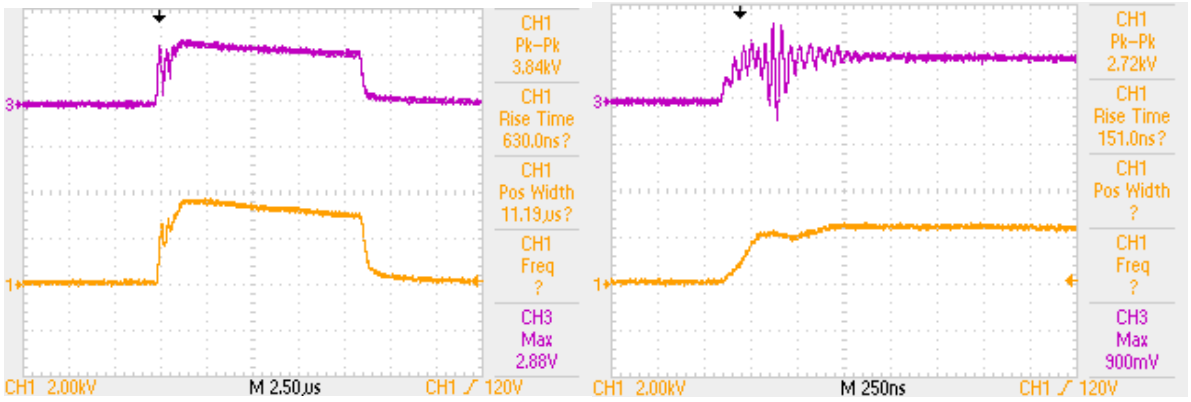

Figure 5.24. Unexpected oscillations during the rise state of the waveform with voltage levels higher than 3.5 kV and with two stages, causing system failure.

A great deal of consideration and experimentation were dedicated to detecting the cause of the failure, such as changing the position of the component, changing the power circuit parameters, and changing the switches and the driver circuit design. However, none of these modifications revealed

the source of the problem, which was, in fact, related to EMI noise generated by the power circuit and the isolating transformers on the IGBT gate signal. It was determined that the failure could be prevented by shielding all the electronic components, such as the driver circuit and its power supply, as shown in Fig. 5.25 and Fig. 5.26. A metallic shield covers the entire electronic circuit and is connected at one point to the circuit's ground.

Figure 5.25. Shielding the IGBT driver circuit in order to reduce noise.

Another modification was the use of twisted wires for the gate signal, as shown in Fig. 5.25. This change reduced the loop inductance and minimized the effect of EMI on the driver circuit. The length of the twisted wires was found not to be critical: changing the length of the wires had no significant effect on the results.

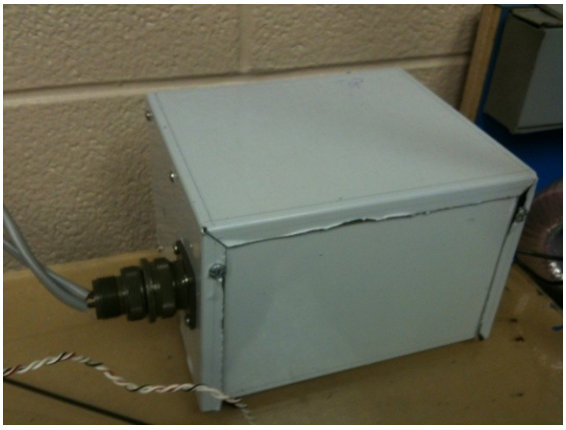

Figure 5.26. Shielding the power supply of the driver circuit in order to reduce noise.

Eliminating an unnecessary ground loop was another factor that had to be taken into account. The ground loop current shown in Fig. 5.27 was eliminated due to its adverse effect on the switching speed, which caused some oscillation at the gate and even false triggering of the switch. All possible ground loops in the generator were eliminated.

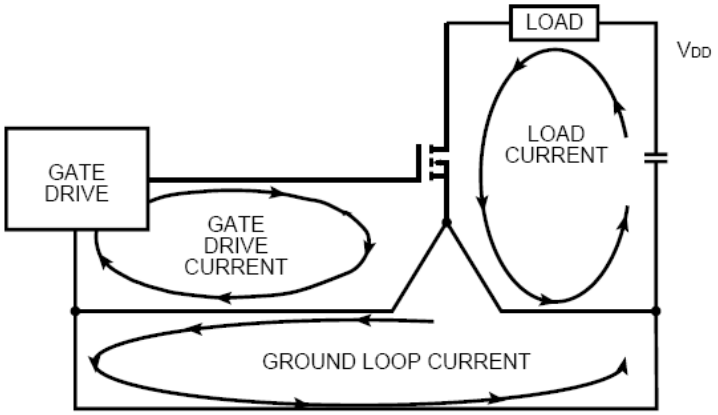

Figure 5.27. Ground loop current in the driver circuit [74].

Chapter 6
Conclusion and Future Works

This chapter provides a summary of the research, the conclusions drawn, and suggestions for future work.

6.1 Summary and Conclusion

The literature cited in Chapter 1 supports the possibility of using PEF as an appropriate alternative method of treating liquid food. The non-thermal nature of the process preserves the nutritional value, colour, and taste of the product during treatment, and its efficiency is greater than that achieved with conventional pasteurization. Developing a pulse generator suitable for the PEF process is therefore an important goal. It was concluded that using a square waveform with an electric field of about 40 kV/cm and a pulse width in the order of microseconds can result in highly efficient food treatment. On the other hand, the generator must be capable of generating a strong current in order to fulfill the requirements associated with liquids. Another important parameter is the flow of the liquid, which is determined by the speed of the switching. Given these considerations, IGBT switches were selected as the best means of meeting these requirements.

The generator was implemented in two stages, based on a Marx generator design. The design allows the voltage to be stepped up using a chain of capacitors charging in parallel and discharging in series, which provides cascade-ability and requires a lower input DC voltage. A 3 kV, 12 A IGBT (IXBH12N300) switch was selected for charging, and a 3 kV, 55 A IGBT (IXBX55N300) switch was selected for discharging. The positive temperature coefficient of these switches allows them to be connected in parallel to enhance the current capability. A TC4421 IGBT driver IC was employed to deliver the control pulses to the IGBT, with an optical isolator connecting the controller to the driver circuit in order to immunize the system from noise. The control unit for generating the desired waveform was based on a PIC microcontroller, which allows the user to set the frequency, pulse width, and test duration using a keypad and LCD interfaces.

To confirm the functionality of the generator, a variety of liquids were subjected to the PEF pulses: pure water, tap water, apple juice, orange juice, apple cider, and tomato juice. Troubleshooting procedures were employed with respect to the generator in order to identify and eliminate any noise that could cause failure during the implementation process. A variety of switches and driver circuits were tested with the goals of finding one suitable for the PEF application and also of enhancing the transient properties of the switches. The effect of pulse width on the temperature rise in the liquid was also investigated in order to determine the best waveform for maximum performance and efficiency. Based on the research, the following conclusions can be drawn:

- The generator is capable of generating up to 6 kV and 1.6 kA using a two-stage generator with two switches in parallel in each stage. It is possible to increase the voltage level by adding more stages and the current level by adding more switches in parallel. Because the current is almost balanced in the parallel switches, no snubber circuits need to be added. The user can set the output pulse width to values from 1 μs to 10 μs.
- Adding more switches in parallel resulted in faster rise/fall times while increasing the number of stages slowed the transients. Eliminating stray inductance was important for keeping the transient times within a reasonable range.
- With respect to the switch gate charge requirement, use of an appropriate driver circuit was important. Increasing the number of driver chips to drive one switch with a higher gate current and faster transient had no significant effect, and a boosted voltage on the gate was needed to push more current to the IGBT. Using switches with a smaller die is another solution for speeding up the rise and fall times; however, it resulted in lower currents.
- Solutions to eliminate EMI noise in the generator included shielding the driver circuit and its power supply, decreasing stray inductance by replacing the wires, rearranging the placement of the high voltage components and electromagnetic radiating devices

in order to prevent interference, using an optical isolator between the signal and power connections, and eliminating ground loops.

- Shorter pulse widths resulted in a lower temperature rise, provided the applied energy was kept constant. This finding means that, for a given flow rate, it is more efficient to increase the frequency of the pulses and to decrease the pulse width.

6.2 Future Work

The following are suggestions for continuing this research with the goal of developing a commercially viable generator for food treatment applications:

- Microbiological tests should be carried out in order to confirm such design parameters as electric field, pulse width, and energy applied.
- The newly developed IGBTs, which are produced for pulsed power applications and are capable of carrying higher voltages with faster rise and fall times, should be tested. The generation of higher voltages by increasing the number of stages could also be explored, treating high conductivity liquids.
- A treatment system should be developed for testing the liquid in both stationary and continuous treatment applications, including the addition of coolers to maintain as low a temperature as possible in the liquid.
- Simulations based on the finite element method could be performed in order to investigate the possibility of decreasing the load current in the chamber by coating the chamber with a material that has a permittivity much higher than that of the liquid.
- To achieve better performance, the driver circuit should be enhanced; one possibility is to increase the gate voltage for faster charging of the gate capacitor.
- Protection from such malfunctions as overvoltage, overcurrent, and desaturation should be added on each switch to prevent system failure in the case of load faults.
- The controller unit could be upgraded to provide more user-friendly options.
- Greater input power should be employed to make it possible to test a system that has higher flow rates.

Bibliography

[1] A. J. H. Sale and W. A. Hamilton, "Effects of high electric fields on microorganisms: I. Killing of bacteria and yeasts," Biochimica Et Biophysica Acta (BBA) - General Subjects, vol. 148, pp. 781-788, 12/27, 1967.

[2] U. Zimmermann, "Electrical breakdown, electropermeabilization and electrofusion," Reviews of Physiology, Biochemistry, and Pharmacology 105, 175-256, 1986.

[3] D. Knorr, M. Geulen, T. Grahl and W. Sitzmann, "Food application of high electric field pulses," Trends Food Sci. Technol., vol. 5, pp. 71-75, 3, 1994.

[4] K. Shamsi and F. Sherkat, "Application of pulsed electric field in non-thermal processing of milk," Asian Journal of Food and Agro-Industry, vol. 2, pp. 216-244, 2009.

[5] K.J. Kinosita and T.Y. Tsong, "Voltage induced pore formation and haemolysis erythrocytes," Biochimica et biophysica acta, vol. 471, pp. 227-242, 1977.

[6] J. C. Weaver, Y. A. Chizmadzhev, "Theory of electroporation: A review," Bioelectrochemistry and Bioenergetics, vol. 41, pp. 135-160, 1996.

[7] A. J. Castro, G. V. Barbosa-Canovas and B. G. Swanson, "Microbial Inactivation of Foods by Pulsed Electric Fields," Journal of Food Processing and Preservation, pp. 47-73, 1993.

[8] V. Heinz, S. Toepfl and D. Knorr, "Impact of temperature on lethality and energy efficiency of apple juice pasteurization by pulsed electric fields treatment," Innovative Food Science & Emerging Technologies, vol. 4, pp. 167-175, 6, 2003.

[9] P. C. Wouters, A. P. Bos and J. Ueckert, " Membrane Permeabilization in Relation to Inactivation Kinetics of Lactobacillus Species due to Pulsed Electric Fields," Applied and Environmental Microbiology, vol. 67, pp. 3092-3101, 2001.

[10] F. Abram, J. P. P. M. Smelt, R. Bos and P. C. Wouters, " Modelling and optimization of inactivation of Lactobacillus plantarum by pulsed electric field treatment," Journal of Applied Microbiology, Blackwell Science Ltd, vol. 94, pp. 571-579, 2003.

[11] A. H. El-Hag, S. H. Jayaram and M. W. Griffiths, "Inactivation of Naturally Grown Microorganisms in Orange Juice Using Pulsed Electric Fields," Plasma Science, IEEE Transactions on, vol. 34, pp. 1412-1415, 2006.

[12] F. Sampedro, A. Rivas, D. Rodrigo, A. Martínez and M. Rodrigo, "Pulsed electric fields inactivation of Lactobacillus plantarum in an orange juice–milk based beverage: Effect of process parameters," J. Food Eng., vol. 80, pp. 931-938, 6, 2007.

[13] L. Salvia-Trujillo, M. Morales-de la Peña, M. A. Rojas-Graü and O. Martín-Belloso, "Microbial and enzymatic stability of fruit juice-milk beverages treated by high intensity pulsed electric fields or heat during refrigerated storage," Food Control, vol. 22, pp. 1639-1646, 10, 2011.

[14] Wei Luo, Ruobing Zhang, Liming Wang, Zhicheng Guan, Zhidong Jia and Xiaojun Liao, "Investigation on shelf life of carrot juice processed by pulse electric field," in High Voltage Engineering and Application, 2008. ICHVE 2008. International Conference on, 2008, pp. 735-741.

[15] G. Pataro, B. Senatore, G. Donsì and G. Ferrari, "Effect of electric and flow parameters on PEF treatment efficiency," J. Food Eng., vol. 105, pp. 79-88, 7, 2011.

[16] J. B. Gurtler, R. B. Bailey, D. J. Geveke and H. Q. Zhang, "Pulsed electric field inactivation of E. coli O157:H7 and non-pathogenic surrogate E. coli in strawberry juice as influenced by sodium benzoate, potassium sorbate, and citric acid," Food Control, vol. 22, pp. 1689-1694, 10, 2011.

[17] G. A. Evrendilek, S. Li, W. R. Dantzer and Q. H. Zhang, "Pulsed Electric Field Processing of Beer: Microbial, Sensory, and Quality Analyses," Journal of Food Science, vol. 69, pp. 228-232, 2004.

[18] A. Gad and S. H. Jayaram, "Electrode Material Migration during Pulsed Electric Field (PEF) Treatment," Proc. ESA Annual Meeting on Electrostatics, 2011.

[19] B. Qin, F. Chang, G. V. Barbosa-Cánovas and B. G. Swanson, "Nonthermal inactivation of Saccharomyces cerevisiae in apple juice using pulsed electric fields," Lebensmittel-Wissenschaft Und-Technologie, vol. 28, pp. 564-568, 7, 1995.

[20] Q. Zhang, A. Monsalve-Gonzalez, B. Qin, G. V. Barbosa-Canovas and B. G. Swanson, "Inactivation of Saccharomyces cerevisiae in Apple Juice by Square-Wave and Exponential Decay Pulsed Electric Fields," Journal of Food Process Engineering, vol. 17, pp. 469-478, 1994.

[21] A. Sobrino-López and O. Martín-Belloso, "Review: Potential of High-Intensity Pulsed Electric Field Technology for Milk Processing," Food Engineering Reviews, vol. 2, pp. 17-27, 2010.

[22] R. Soliva-Fortuny, A. Balasa, D. Knorr and O. Martín-Belloso, "Effects of pulsed electric fields on bioactive compounds in foods: a review," Trends Food Sci. Technol., vol. 20, pp. 544-556, 12, 2009.

[23] M. Sack, J. Sigler, C. Eing, L. Stukenbrock, R. Stangle, A. Wolf and G. Muller, "Operation of an electroporation device for grape mash," in 2010, pp. 1928-1934.

[24] Y. Chalermchat and P. Dejmek, "Effect of pulsed electric field pretreatment on solid-liquid expression from potato tissue," J. Food Eng., vol. 71, pp. 164-169, 2005.

[25] M. I. Bazhal, N. I. Lebovka and E. Vorobiev, "Pulsed electric field treatment of apple tissue during compression for juice extraction," J. Food Eng., vol. 50, pp. 129-139, 2001.

[26] M. Fincan, F. DeVito and P. Dejmek, "Pulsed electric field treatment for solid-liquid extraction of red beetroot pigment," J. Food Eng., vol. 64, pp. 381-388, 2004.

[27] N. Lopez, E. Puertolas, S. Condon, J. Raso and I. Alvarez, "Enhancement of the solid-liquid extraction of sucrose from sugar beet (Beta vulgaris) by pulsed electric fields," LWT - Food Science and Technology, vol. 42, pp. 1674-1680, 2009.

[28] F. Sampedro, D. Rodrigo, A. Martinez, G. Barbosa-Canovas and M. Rodrigo, "Review: Application of pulsed electric fields in egg and egg derivatives," Food Sci. Technol. Int., vol. 12, pp. 397-406, 2006.

[29] M. Amiali, M. O. Ngadi, V. G. S. Raghavan and J. P. Smith, "Inactivation of Escherichia coli O157:H7 in liquid dialyzed egg using pulsed electric fields," Food Bioprod. Process., vol. 82, pp. 151-156, 2004.

[30] S. Monfort, E. Gayan, G. Saldana, E. Puertolas, S. Condon, J. Raso and I. Alvarez, "Inactivation of Salmonella Typhimurium and Staphylococcus aureus by pulsed electric fields

in liquid whole egg," Innovative Food Science and Emerging Technologies, vol. 11, pp. 306-313, 2010.

[31] I. Alvarez, R. Pagan, S. Condon, J. Raso, The influence of process parameters for the inactivation of Listeria monocytogenes by pulsed electric fields, International Journal of Food Microbiology, Volume 87, Issues 1-2, 15 October 2003, Pages 87-95, ISSN 0168-1605, DOI: 10.1016/S0168-1605(03)00056-4.

[32] L. I. Gallo, A. M. R. Pilosof and R. J. Jagus, "Effect of the sequence of nisin and pulsed electric fields treatments and mechanisms involved in the inactivation of Listeria innocua in whey," J. Food Eng., vol. 79, pp. 188-193, 2007.

[33] M. Gudmundsson and H. Hafsteinsson, "Effect of electric field pulses on microstructure of muscle foods and roes," Trends in Food Science and Technology, vol. 12, pp. 122-128, 2001.

[34] Y. Matsumoto, N. Shioji, T. Satake and A. Sakuma, "Inactivation of microorganisms by pulsed high voltage application," in Industry Applications Society Annual Meeting, Conference Record of the 1991 IEEE, vol.1, pp. 652-659, 1991.

[35] Y. Creyghton, R. Beurskens, A. Fiala and S. W. H. de Haan, "Power source for inactivation of micro-organisms with partial high voltage discharge in a continuous process," in Power Modulator Symposium, 2002 and 2002 High-Voltage Workshop. Conference Record of the Twenty-Fifth International, pp. 657-661, 2002.

[36] Q. Zhang, G. V. Barbosa-Canovas and B. G. Swanson, "Engineering Aspect of Pulsed Electric Field Pasteurization," Journal of Food Process Engineering, pp. 261-281, 1995.

[37] A. H. El-Hag, S. H. Jayaram, M. W. Griffths and R. Dadarwal, "Survivability of inoculated versus naturally grown bacteria in liquid foods under pulsed electric fields," in Industry Applications Society Annual Meeting, 2008. IAS '08. IEEE, 2008, pp. 1-4.

[38] A. H. El-Hag, S. H. Jayaram, O. Rodriguez and M. Griffiths, "A performance study of a multi-level electrode treatment chamber for food processing," in Industry Applications Society Annual Meeting (IAS), 2010 IEEE, 2010, pp. 1-4.

[39] S. Toepfl, V. Heinz and D. Knorr, "High intensity pulsed electric fields applied for food preservation," Chem. Eng. Process, vol. 46, pp. 537-546, 6, 2007.

[40] S. W. H. de Haan and P. R. Willcock, "Comparison of the energy performance of pulse generation circuits for PEF," Innovative Food Science & Emerging Technologies, vol. 3, pp. 349-356, 12, 2002.

[41] J. R. Beveridge, S. J. MacGregor, J. G. Anderson and R. A. Fouracre, "The Influence of Pulse Duration on the Inactivation of Bacteria Using Monopolar and Bipolar Profile Pulsed Electric Fields," Plasma Science, IEEE Transactions on, vol. 33, pp. 1287-1293, 2005.

[42] S. H. Jayaram, A. H. El-Hag, F. P. Espino-Cortes, R. J. Wong and C. Leibovitch, "Effects of process and product parameters on the shape of nanosecond pulses used in high-field liquid food treatment," Industry Applications, IEEE Transactions on, vol. 41, pp. 520-526, 2005.

[43] B. M. Novac, P. Sarkar, I. R. Smith, W. Whittow and C. Greenwood, "An innovative and non-invasive technology for PEF food processing," in Pulsed Power Conference, 2009. PPC '09. IEEE, 2009, pp. 737-741.

[44] R. Narsetti, R. D. Curry, K. F. McDonald, L. M. Nichols and T. Clevenger, "Application of pulsed electric fields and magnetic pulse compressor technology for water sterilization," in Pulsed Power Conference, 2005 IEEE, 2005, pp. 1282-1285.

[45] Y. Chang, S. Tseng, T. Wu and H. Yang, "Narrow pulsed electric field generator using forward / flyback hybrid converters for liquid food processing," in Sustainable Energy Technologies, 2008. ICSET 2008. IEEE International Conference on, 2008, pp. 910-915.

[46] J. R. Grenier, S. H. Jayaram, M. Kazerani, Haifeng Wang and M. W. Griffiths, "MOSFET-Based Pulse Power Supply for Bacterial Transformation," Industry Applications, IEEE Transactions on, vol. 44, pp. 25-31, 2008.

[47] S. Tseng, T. Wu, H. Yang, J. Guo and J. Hung, "Soft-switching series-resonant converter to generate high output voltage for processing microbes," in Applied Power Electronics Conference and Exposition, 2004. APEC '04. Nineteenth Annual IEEE, 2004, pp. 905-911 vol.2.

[48] C. Wang, Q. H. Zhang and C. Streaker, "A 12 kV solid state high voltage pulse generator for a bench top PEF machine," in Power Electronics and Motion Control Conference, 2000. Proceedings. IPEMC 2000. the Third International, 2000, pp. 1347-1352 vol.3.

[49] Ju-Won Baek, Dong-Wook Yoo and Geun-Hie Rim, "Solid state marx generator using series-connected IGBTs," in Power Modulator Symposium, 2004 and 2004 High-Voltage Workshop. Conference Record of the Twenty-Sixth International, 2004, pp. 383-386.

[50] S. A. Ghani, W. I. Ibrahim, M. R. Ghazali and N. A. Azli, "Power electronics converter with marx generator configuration based PEF for liquid food sterilization," in Electrical, Control and Computer Engineering (INECCE), 2011 International Conference on, 2011, pp. 416-419.

[51] M. P. J. Gaudreau, T. Hawkey, J. Petry and M. A. Kempkes, "A solid state pulsed power system for food processing," in Pulsed Power Plasma Science, 2001. PPPS-2001. Digest of Technical Papers, 2001, pp. 1174-1177 vol.2.

[52] M. Gaudreau, T. Hawkey, J. Petry and M. Kempkes, "Solid-state power systems for pulsed electric field (PEF) processing," in Pulsed Power Conference, 2005 IEEE, 2005, pp. 1278-1281.

[53] G. Belverde, A. Galluzzo, M. Melito, S. Musumeci and A. Raciti, "Snubberless voltage sharing of series-connected insulated-gate devices by a novel gate control strategy," Power Electronics, IEEE Transactions on, vol. 16, pp. 132-141, 2001.

[54] V. Chitta, Soonwook Hong and D. A. Torrey, "Series connection of IGBTs with active voltage balancing," in Industry Applications Conference, 1997. Thirty-Second IAS Annual Meeting, IAS '97., Conference Record of the 1997 IEEE, 1997, pp. 961-967 vol.2.

[55] P. R. Palmer and A. N. Githiari, "The series connection of IGBTs with active voltage sharing," Power Electronics, IEEE Transactions on, vol. 12, pp. 637-644, 1997.

[56] A. Piazzesi and L. Meysenc, "Series connection of 3.3 kV IGBTs with active voltage balancing," in Power Electronics Specialists Conference, 2004. PESC 04. 2004 IEEE 35th Annual, 2004, pp. 893-898 Vol.2.

[57] H. A. Prins, R. H. S. H. Beurskens, Y. L. M. Creyghton, N. Dutreux, S. W. H. de Haan and B. Roodenburg, "Solid state pulsed power source for pulsed electric field and plasma treatment of food products," in Pulsed Power Plasma Science, 2001. PPPS-2001. Digest of Technical Papers, 2001, pp. 1294-1297 vol.2.

[58] S. H. Jayaram, "Pulsed Power Applied to Process Industry," Industry Applications Magazine, IEEE, vol. 16, pp. 34-40, 2010.

[59] S. Jayaram and K. L. Rao, "Treatment Chamber for Non-thermal Pasteurization of Liquid Foods using Pulsed Electric Field," Patent Corporation Treaty (PCT), International Publication Number, WO 2005/107821 A1.

[60] Mohan, Ned; Undeland, Tore M.; Robbins, William P. (2003). Power Electronics - Converters, Applications, and Design (3rd Edition). John Wiley & Sons. Online version available at: http://www.knovel.com/web/portal/browse/display?_EXT_KNOVEL_DISPLAY_bookid=3400&VerticalID=0.

[61] Data sheet: IXBX55N300. Available at web site: www.IXYS.com.

[62] Data sheet: CM600HA-24A. Available web site: www.pwrx.com.

[63] Available at web site: http://www.aqon-gmbh.com/products/AQON-Pulsed-Electric-Field-Technology.

[64] Bai-Lin Qin, Qinghua Zhang, G. V. Barbosa-Canovas, B. G. Swanson and P. D. Pedrow, "Inactivation of microorganisms by pulsed electric fields of different voltage waveforms," Dielectrics and Electrical Insulation, IEEE Transactions on, vol. 1, pp. 1047-1057, 1994.

[65] S. Toepfl, A. Mathys, V. Heinz and Knorr, "Review: potential of high hydrostatic pressure and pulsed electric fields for energy efficient and environmentally friendly food processing," Food Reviews International, vol.22, pp. 405–423, 2006.

[66] Y. Yu, "High Voltage Square-Wave and SPWM-Wave Generator Design and Application," ECE Dept. University of Waterloo, Waterloo, Ontario, Canada, MACs Thesis, 2009.

[67] Data sheet: TD351. Available at web site: www.st.com.

[68] Data sheet: TC4421. Available at web site: www.microchip.com.

[69] Data sheet: MIC4451. Available at web site: www.micrel.com.

[70] Application note: AN786, Driving Power MOSFETs in High-Current, Switch Mode Regulators. Available at web site: www.microchip.com.

[71] M. N. Nguyen, R. L. Cassel, J. E. deLamare and G. C. Pappas, "Gate drive for high speed, high power IGBTs," in Pulsed Power Plasma Science, 2001. PPPS-2001. Digest of Technical Papers, 2001, pp. 1039-1042 vol.2.

[72] Data sheet: 16F87xA. Available at web site: www.microchip.com.

[73] B. Roodenburg, J. Morren, H. E. Berg and S. W. H. de Haan, "Metal Release in a Stainless Steel Electric Field (PEF) System – Part I. Effect of Different Pulse Shapes; Theory and Experimental Method," Innovative Food Science and Emerging Technologies, Vol. 6, pp. 327-336, 2005.

[74] Application note: APT9302, Gate Drive Design for Large Die MOSFETs. Available at web site: www.nalanda.nitc.ac.in.